Homeostatic Synaptic Plasticity of Miniature Excitatory Postsynaptic Currents in Mouse Cortical Cultures Requires Neuronal Rab3A.

Andrew G. Koesters[1*], Mark M. Rich[2], and Kathrin L. Engisch[3]

[1]Department of Pharmacology and Systems Physiology, University of Cincinnati College of Medicine, Cincinnati, OH 45267, USA
[2]Department of Neuroscience, Cell Biology and Physiology, Boonshoft School of Medicine, Wright State University, Dayton, OH 45345
[3]Department of Neuroscience, Cell Biology and Physiology, Boonshoft School of Medicine and the College of Science and Mathematics, Wright State University, Dayton, OH 45435

*Andrew G. Koesters –Corresponding author
Department of Pharmacology and Systems Physiology, University of Cincinnati College of Medicine, Cincinnati, OH 45267, USA
koesteag@ucmail.uc.edu, ph 513-558-2819

Author contributions: A.G.K., K.L.E. and M.M.R. designed research; A.G.K. performed research; A.G.K. and K.L.E. analyzed data; A.G.K, K.L.E., and M.M.R. wrote the paper.

ORCID iDs: ; A.G.K, https://orcid.org/0000-0003-3281-188X; M.M.R., https://orcid.org/0000-0002-6956-5531; K.L.E., https://orcid.org/0000-0002-1058-5343

The authors have no competing interests.

Keywords: Homeostatic Synaptic Plasticity; Synaptic Scaling; mEPSCs; Rab3A; AMPA receptors

28 Abstract

29 Following prolonged activity blockade, amplitudes of miniature excitatory postsynaptic currents
30 (mEPSCs) increase, a form of homeostatic plasticity termed "synaptic scaling." We previously
31 showed that a presynaptic protein, the small GTPase Rab3A, is required for full expression of
32 the increase in miniature endplate current amplitudes following prolonged blockade of action
33 potential activity at the mouse neuromuscular junction in vivo (Wang et al., 2011), but it is
34 unknown whether this form of Rab3A-dependent homeostatic plasticity shares any
35 characteristics with central synapses. We show here that synaptic scaling of mEPSCs is impaired
36 in mouse cortical neuron cultures prepared from Rab3A$^{-/-}$ and Rab3A Earlybird mutant mice. To
37 determine if Rab3A is involved in the well-established homeostatic increase in postsynaptic
38 AMPA-type receptors (AMPARs), we performed a series of experiments in which
39 electrophysiological recordings of mEPSCs and confocal imaging of synaptic AMPAR
40 immunofluorescence were assessed within the same cultures. We found that Rab3A is required
41 for the increase in synaptic AMPARs following prolonged activity blockade, but the comparison
42 of mEPSC amplitude and synaptic AMPARs in the same cultures revealed that mEPSC amplitude
43 cannot solely be determined by postsynaptic AMPAR levels. Finally, we demonstrate that
44 Rab3A is acting in neurons because selective loss of Rab3A in astrocytes did not disrupt
45 homeostatic plasticity, whereas selective loss in neurons strongly reduced the homeostatic
46 increase in mEPSC amplitudes. Taken together with the results at the neuromuscular junction,
47 we propose that Rab3A is a presynaptic homeostatic regulator that controls quantal size on
48 both sides of the synapse.

Introduction

One of the most studied phenomena triggered by prolonged activity blockade is the increase in amplitudes of miniature excitatory postsynaptic currents (mEPSCs), first demonstrated in cultures of dissociated cortical neurons (Turrigiano et al., 1998) and spinal cord neurons (O'Brien et al., 1998). This compensatory response is now termed homeostatic synaptic plasticity (Turrigiano and Nelson, 2004; Pozo and Goda, 2010) and has been shown to be dysregulated in several neurodevelopment, psychiatric, and neurodegenerative disorders. One of the initial studies of homeostatic synaptic plasticity demonstrated that AMPAergic mEPSCs were uniformly increased after prolonged activity blockade (Turrigiano et al., 1998), and the authors named this process synaptic scaling. An accompanying increase in AMPA-type glutamate receptors (AMPARs) was observed in both of the early studies of homeostatic synaptic plasticity (O'Brien et al., 1998; Turrigiano et al., 1998), and has been confirmed many times (a non-exhaustive list includes (Ju et al., 2004; Thiagarajan et al., 2005; Shepherd et al., 2006; Stellwagen and Malenka, 2006; Hou et al., 2008; Gainey et al., 2009; Soden and Chen, 2010; Correa et al., 2012; Altimimi and Stellwagen, 2013; Letellier et al., 2014; Xu and Pozzo-Miller, 2017).

Homeostatic synaptic plasticity is becoming increasingly implicated in both pathological brain conditions, for example, epilepsy, neuropsychiatric disorders, Huntington's, and alcohol use disorder (Trasande and Ramirez, 2007; Fernandes and Carvalho, 2016; Wang et al., 2017; Lovinger and Abrahao, 2018; Smith-Dijak et al., 2019; Lignani et al., 2020; Suzuki et al., 2021; Kavalali and Monteggia, 2023), and essential normal functions such as sleep (Tononi and Cirelli, 2014; Diering et al., 2017; Torrado Pacheco et al., 2021), so a molecular understanding of the

71 process is an extremely important next step. The homeostatic synaptic plasticity field has
72 identified several proteins required for synaptic scaling of mEPSC amplitudes, the majority of
73 which are involved in the regulation of AMPAR levels (Shepherd et al., 2006; Seeburg and
74 Sheng, 2008; Gao et al., 2010; Anggono et al., 2011; Beique et al., 2011; Diering et al., 2014;
75 Gainey et al., 2015; Tan et al., 2015; Pastuzyn and Shepherd, 2017; Sanderson et al., 2018).

76 In our previous work studying the increase in miniature endplate currents (mEPC)
77 following prolonged in vivo activity-block of synaptic transmission at the mouse neuromuscular
78 junction (NMJ), we were surprised to find no evidence of changes in acetylcholine receptor
79 (AChR) levels (Wang et al., 2005). This result led us to search for presynaptic molecules that
80 might homeostatically regulate mEPC amplitude, perhaps via the presynaptic quantum. In
81 previous studies in chromaffin cells, we identified the small GTPase Rab3A, a synaptic vesicle
82 protein, as a regulator of synaptic vesicle fusion pore opening (Wang et al., 2008), so we
83 examined whether deletion of Rab3A (Rab3A$^{-/-}$) might prevent homeostatic upregulation of
84 mEPC amplitude. The results were clear: in the Rab3A$^{-/-}$ mouse, the homeostatic increase in
85 mEPC amplitude was strongly reduced, and was completely abolished in mice expressing a
86 point mutation in Rab3A, the Earlybird mutant (Rab3A$^{Ebd/Ebd}$) (Wang et al., 2011).

87 The Rab3A$^{-/-}$ mouse has minimal phenotypic abnormalities, with evoked synaptic
88 transmission and mEPSCs essentially normal in hippocampal slices (Geppert et al., 1994). At the
89 Rab3A$^{-/-}$ NMJ, reductions in evoked transmission were detected, but only under conditions of
90 reduced extracellular calcium (Coleman et al., 2007). The most dramatic effect of loss of Rab3A
91 is the disruption of a presynaptic form of long-term potentiation (LTP) at the mossy fiber-CA3
92 synapse (Weisskopf et al., 1994; Castillo et al., 1997). To our knowledge, there is no evidence of

93 Rab3A involvement in the expression or trafficking of postsynaptic receptors. Our results at the
94 mammalian NMJ suggest that in addition to its importance in mossy fiber LTP, Rab3A may be
95 required for the homeostatic plasticity of mEPSC amplitude via a presynaptic mechanism.

96 In the current work, we explored whether the in vivo findings at the NMJ might also
97 apply to the more typically studied homeostatic synaptic plasticity of mEPSC amplitude in
98 dissociated cortical neuron cultures. We report that our findings in vivo at the NMJ were almost
99 exactly recapitulated in cultures of dissociated cortical neurons: 1. strong reduction of the
100 homeostatic increase in mEPSC amplitude in the absence of Rab3A; 2. complete abolishment of
101 the homeostatic increase in mEPSC amplitude in the presence of the Rab3A Earlybird mutant;
102 and 3. increased mEPSC amplitude in the Rab3A Earlybird mutant prior to activity blockade.
103 However, in contrast to the unchanged AChR levels at the mammalian NMJ, there was a
104 modest increase in levels of the GluA2-type AMPARs at cortical synapses after activity-
105 blockade, which appeared to be disrupted in cultures prepared from Rab3A$^{-/-}$ mice.
106 Importantly, when compared within the same cultures, GluA2 receptor levels did not always
107 parallel mEPSC amplitudes. We also determined that Rab3A must be present in neurons, but
108 not astrocytes, for full expression of homeostatic plasticity. The NMJ and cortical culture data
109 taken together strongly suggest neuronal Rab3A is important for both postsynaptic receptor
110 upregulation and a second mechanism affecting mEPSC amplitude, likely the amount of
111 transmitter released by a single vesicle.

112

113 <u>Materials and Methods</u>

114 *Animals.* Rab3A$^{+/-}$ heterozygous mice were bred and genotyped as previously described
115 (Kapfhamer et al., 2002; Wang et al., 2008). Rab3A$^{Ebd/Ebd}$ mice were identified in an EU-
116 mutagenesis screen of C57BL/6J mice, and after a cross to C3H/HeJ, were backcrossed for 3
117 generations to C57BL/6J (Kapfhamer et al., 2002). Rab3A$^{+/Ebd}$ heterozygous mice were bred at
118 Wright State University and genotyped in a two-step procedure: 1. a PCR reaction with RabF1
119 and Dcaps3R as primers; and 2. a digestion with enzyme Bsp1286I (New England Biolabs) that
120 distinguishes the Earlybird mutant by its different base-pair products. Rab3A$^{+/-}$ mice were
121 backcrossed with Rab3A$^{+/+}$ mice from the Earlybird heterozygous colony for 11 generations in
122 an attempt to establish a single wild type strain, but differences in mEPSC amplitude and
123 adrenal chromaffin cell calcium currents persisted, likely due to genes that are close to the
124 Rab3A site, resulting in two wild type strains: 1. Rab3A$^{+/+}$ from the Rab3A$^{+/-}$ colony, and 2.
125 Rab3A$^{+/+}$ from the Rab3A$^{+/Ebd}$ colony.

126 *Primary Culture of Mouse Cortical Neurons.* Primary dissociated cultures of mixed neuronal and
127 astrocyte populations were prepared as previously described (Hanes et al., 2020). Briefly,
128 postnatal day 0-2 (P0-P2) Rab3A$^{+/+}$, Rab3A$^{-/-}$ or Rab3A$^{Ebd/Ebd}$ neonates were euthanized by rapid
129 decapitation, as approved by the Wright State University Institutional Animal Care and Use
130 Committee, and brains were quickly removed. Each culture was prepared from the cortices
131 harvested from two animals; neonates were not sexed. Cortices were collected in chilled
132 Neurobasal-A media (Gibco) with osmolarity adjusted to 270 mOsm and supplemented with 40
133 U/ml DNAse I (ThermoFisher Scientific). The tissues were digested with papain (Worthington
134 Biochemical) at 20 U/ml at 37°C for 20 minutes followed by trituration with a sterile, fire-
135 polished Pasteur pipette, then filtered through a 100 μm cell strainer, and centrifuged at 1100

136 rpm for 2 minutes. After discarding the supernatant, the pellet was resuspended in room
137 temperature Neurobasal-A media (270 mOsm), supplemented with 5% fetal bovine serum for
138 astrocyte growth, and 2% B-27 supplement to promote neuronal growth (Gibco), L-glutamine,
139 and gentamicin (ThermoFisher Scientific). Neurons were counted and plated at $0.15 * 10^6$
140 cells/coverslip onto 12 mm coverslips pre-coated with poly-L-lysine (BioCoat, Corning). The
141 culture media for the first day (0 DIV) was the same as the above Neurobasal-A media
142 supplemented with FBS, B-27, L-glutamine, and gentamicin, and was switched after 24 hours (1
143 DIV) to media consisting of Neurobasal-A (270 mOsm), 2% B-27, and L-glutamine without FBS to
144 avoid its toxic effects on neuronal viability and health (Stellwagen and Malenka, 2006). Half of
145 the media was changed twice weekly and experiments were performed at 13-14 DIV. Two days
146 prior to experiments, tetrodotoxin (TTX) (500 nM; Tocris), a potent Na^+ channel blocker, was
147 added to some cultures to chronically silence all network activity and induce homeostatic
148 synaptic plasticity mechanisms, while untreated sister cultures served as controls. Cultures
149 prepared from mutant mice were compared with cultures from wild-type mice from their
150 respective colonies. Note that the cultures comprising the $Rab3A^{+/+}$ data here are a subset of
151 the data previously published in Hanes et al., 2020, and therefore the plots in Figure 1 are not
152 identical to those in the previously published work. This smaller data set was restricted to the
153 time period over which cultures were prepared from $Rab3A^{-/-}$ mice.

154 *Preparation of Astrocyte Feeder Layers.* Astrocyte feeder layers were prepared from the
155 cortices of P0-P2 $Rab3A^{+/+}$ or $Rab3A^{-/-}$ mouse pups as described previously (Stellwagen and
156 Malenka, 2006). Briefly, cortices were dissected and cells were dissociated as described above.
157 Cell suspensions of mixed neuronal and astrocyte populations were plated onto glass coverslips

158 pre-coated with poly-L-lysine in Dulbecco's Modified Eagle Media (ThermoFisher Scientific)
159 supplemented with 5% FBS (to promote astrocyte proliferation and to kill neurons), L-
160 glutamine, and gentamicin, and maintained in an incubator at 37°C, 5% CO_2; cultures were
161 maintained in this manner for up to 1 month to generate purely astrocytic cultures (all neurons
162 typically died off by 7 DIV). Culture media was replaced after 24 hours, and subsequent media
163 changes were made twice weekly, replacing half of the culture media with fresh media. Feeder
164 layers were not used for neuronal seeding until all native neurons were gone and astrocytes
165 approached 100% confluency (visually inspected).
166 *Plating of Neurons on Glial Feeder Layers.* Cortical neurons were obtained as described above.
167 The cell pellet obtained was resuspended in Neurobasal-A (osmolarity adjusted to 270 mOsm)
168 containing B27 (2%, to promote neuronal growth), L-glutamine, and 5-fluorodeoxyuridine (FdU,
169 a mitotic inhibitor; Sigma). Addition of FdU was used to prevent astrocyte proliferation and
170 contamination of the feeder layer with new astrocytes, promoting only neuronal growth on the
171 feeder layers (FdU-containing media was used for the maintenance of these cultures and all
172 subsequent media changes). Astrocyte culture media was removed from the feeder layer
173 cultures, and the neuronal cell suspension was plated onto the astrocyte feeder cultures. The
174 culture strategy used to distinguish the relative roles of neuronal and astrocytic Rab3A is
175 outlined in Figure 9. At 1 DIV, all of the culture media was removed and replaced with fresh
176 Neurobasal-A media containing FdU described above, and half of the media was replaced twice
177 per week for all subsequent media changes. Cultures were maintained in a 37°C, 5% CO_2
178 incubator for 13-14 DIV.

179 *Whole-Cell Voltage Clamp to Record mEPSCs*. At 13-14 DIV, mEPSCs from TTX-treated and
180 untreated sister cultures of Rab3A$^{+/+}$ or Rab3A$^{-/-}$ neurons from the Rab3A$^{+/-}$ colony, or Rab3A$^{+/+}$
181 or Rab3A$^{Ebd/Ebd}$ neurons from the Rab3A$^{+/Ebd}$ colony, were recorded via whole-cell voltage clamp
182 to assess the role of Rab3A in homeostatic synaptic plasticity. Recordings were taken from
183 pyramidal neurons, which were identified visually by a prominent apical dendrite; images were
184 taken of all cells recorded from. Cells were continuously perfused with a solution consisting of
185 (in mM): NaCl (115), KCl (5), $CaCl_2$ (2.5), $MgCl_2$ (1.3), dextrose (23), sucrose (26), HEPES (4.2),
186 pH = 7.2 (Stellwagen and Malenka, 2006). On the day of recording, the osmolarity of the media
187 from the cultures was measured (normally 285 – 295 mOsm) and the perfusate osmolarity was
188 adjusted to match the culture osmolarity, to protect against osmotic shock to the neurons. To
189 isolate glutamatergic mEPSCs, TTX (500 nM) and picrotoxin (50 μM) were included in the
190 perfusion solution to block action potentials and GABAergic currents, respectively. The NMDA
191 receptor antagonist, APV, was not included in the perfusion solution because all mEPSCs were
192 blocked by CNQX and picrotoxin, demonstrating no APV-sensitive mEPSCs were present (data
193 not shown). Patch electrodes (3.5 – 5 MΩ) were filled with an internal solution containing (in
194 mM): K-gluconate (128), NaCl (10), EGTA (1), $CaCl_2$ (0.132), $MgCl_2$ (2), HEPES (10), pH = 7.2.
195 Osmolarity was adjusted to 10 mOsm less than the perfusion solution osmolarity. Neurons
196 were clamped at a voltage of -60 mV using an Axopatch 200B patch-clamp (Axon Instruments),
197 recorded from for 2 – 5 minutes, and data were collected with Clampex 10.0/10.2 (Axon
198 Instruments). The antagonist of Ca^{2+}-permeable AMPA receptors (including GluA1 but not
199 GluA2), N-naphthyl acetylspermine (NASPM, 20 μM; Tocris), was applied during recordings in a
200 subset of experiments. Because NASPM is an open channel blocker, it was applied with a

201 depolarizing high K^+ solution (25 mM KCl, 95 mM NaCl). Baseline recordings were performed for
202 2 minutes in our standard perfusate, then were suspended while NASPM + High K^+ solution was
203 applied for 45 seconds, followed by a NASPM only solution for 5 minutes, after which recording
204 was recommenced for 5 minutes (because we found in pilot experiments that frequency was
205 reduced following NASPM application).

206 *Data Analysis and Statistics of mEPSCs.* Miniature excitatory postsynaptic currents were
207 manually selected using Mini Analysis software (Synaptosoft) to identify mEPSCs. The program
208 threshold was set at 3 pA but the smallest mEPSC selected was 4.01 pA. Records were filtered
209 at 2 kHz using a low-pass Butterworth filter prior to selection. For computing mEPSC mean in
210 each experimental condition, individual cell means were pooled across multiple cultures and
211 compared with the non-parametric Kruskal-Wallis test, with n = the number of cells and the
212 overall means presented as ± SEM. For cumulative probability distribution functions (CDFs) of
213 mEPSC amplitude, 30 quantiles were computed for each cell and pooled across cultures (see
214 (Hanes et al., 2020)), and a Kolmogorov-Smirnov test (KS test) was used to test for significant
215 differences, with n = the number of mEPSC quantiles. The rank order plots were created by
216 computing a matched number of quantiles from the two experimental conditions (usually
217 control (CON) and TTX). We used an algorithm to identify the product closest to, but above, 24
218 quantiles for a data set. For example, if there were 13 CON cells and 12 TTX cells, we computed
219 24 quantiles for each of the 13 cells and 26 quantiles for each of the 12 cells, for an equal total
220 number of 312 quantiles for both data sets. The quantiles were sorted from smallest to largest,
221 TTX amplitudes plotted vs. CON amplitudes, and the relationship fit with a linear regression

222 function with the intercept term allowed to vary. The ratio plots were created by taking the
223 ratio of TTX/CON and plotting as a function of the CON amplitude quantiles.
224 *Immunocytochemistry, microscopy, and data analysis.* Primary cultures of mouse cortical
225 neurons were grown for 13-14 DIV. Antibodies to GluA2 (mouse ab against N-terminal, EMD
226 Millipore) were added directly to live cultures at 1:40 dilution, and incubated at 37 °C in a CO_2
227 incubator for 45 minutes. Cultures were rinsed 3 times with PBS/5% donkey serum before being
228 fixed with 4% paraformaldehyde. After 3 rinses in PBS/5% donkey serum, cultures were
229 incubated in CY3-labeled donkey-anti-mouse secondary antibodies for 1 hour at room
230 temperature, rinsed in PBS/5% donkey serum, permeabilized with 0.2% saponin, and incubated
231 in chick anti-MAP2 (1:2500, AbCAM) and rabbit anti-VGLUT1 (1:4000, Synaptic Systems) for 1
232 hour at room temperature in PBS/5% donkey serum. After rinsing with PBS/5% donkey serum,
233 coverslips were incubated with 488-anti chick and CY5-anti rabbit secondary antibodies for 1
234 hour at room temperature, rinsed, blotted to remove excess liquid, and inverted on a drop of
235 Vectashield (Vector Labs). Coverslips were sealed with nail polish and stored at 4 °C for < 1
236 week before imaging. All secondary antibodies were from Jackson Immunoresearch and were
237 used at 1:225 dilution.
238 Coverslips were viewed on a Fluoview FV1000 laser scanning confocal microscope with a
239 60x oil immersion, 1.35 NA objective. Once a pyramidal neuron was identified, Fluoview 2.1
240 software was used to zoom in on the primary dendrite (5X) and confocal sections were taken
241 every 0.5 μm. Images were analyzed offline with ImagePro 6 (Cybernetics). The composite
242 image was used to locate synaptic sites containing both VGLUT1 and GluA2 immunoreactivity in
243 close apposition to each other and to the primary dendrite or a secondary branch. An area of

244 interest (AOI) was manually drawn around the receptor cluster in the confocal section in which
245 it was the brightest. The AOIs for a dendrite were saved in a single file; the AOI number and the
246 confocal section it was associated with were noted for later retrieval. For quantification, AOIs
247 were loaded, an individual AOI was called up on the appropriate section, and the
248 count/measurement tool used to apply a threshold (400 or 450; identical for CON and TTX
249 coverslips but different for different cultures); pixels within the cluster that were above the
250 threshold were automatically outlined, and size, average intensity, and integral of the outlined
251 region reported. For quantile sampling, only dendrites with a minimum of 6 synaptic sites were
252 included. For creating CDFs, 30 quantiles were computed for each dendrite. For the rank order
253 and ratio plots, we matched the total quantiles for CON and TTX GluA2 receptor characteristics
254 as was done above for mEPSC amplitudes.

255

256 Results

257 We previously reported that mixed cultures of cortical neurons and astrocytes prepared
258 from postnatal day 0-2 mouse pups responded to a block of action potential-mediated activity
259 by a 48 hour TTX treatment with an increase in mEPSC amplitude (Hanes et al., 2020). Here, we
260 asked the question whether cortical cultures prepared from mice lacking the small GTPase
261 Rab3A, or, expressing a point mutation of Rab3A, Rab3A Earlybird, have an altered homeostatic
262 plasticity response to a loss of network activity. To obtain Rab3A$^{-/-}$ and Rab3A$^{Ebd/Ebd}$
263 homozygotes, we established two mouse colonies of heterozygous breeders with cultures
264 prepared from pups derived from a final breeding pair of homozygotes. Although we

265 backcrossed Rab3A$^{+/-}$ with Rab3A$^{+/Ebd}$ for 11 generations, clear differences in mEPSC amplitudes
266 in untreated cultures (see below) and in calcium current amplitudes in adrenal chromaffin cells
267 (unpublished obs.) remained. Therefore, throughout this study we keep the two strains
268 separate and there are two Rab3A$^{+/+}$ or 'wild type' phenotypes.

269 Example current traces of spontaneously occurring mEPSCs recorded from pyramidal
270 neurons in untreated (CON) 13-14 DIV cortical cultures and sister cultures treated with 500 nM
271 TTX for 48 hours prepared from wild type animals in the Rab3A$^{+/-}$ colony are shown in Figure
272 1A. Average mEPSC waveforms from the same recordings are shown in Figure 1B. The mean
273 mEPSC amplitudes for 30 control and 23 TTX-treated neurons are displayed in the box and
274 whisker plot in Figure 1C; after activity blockade the average mEPSC amplitude increased from
275 13.9 ± 0.7 pA to 18.2 ± 0.9 pA ($p = 4.58 * 10^{-4}$, Kruskal-Wallis test). Example current traces of
276 mEPSCs and average mEPSC waveforms are shown in Figures 1D and E, respectively, for cortical
277 cultures prepared from Rab3A$^{-/-}$ mice. In contrast to the behavior of neurons in cultures
278 prepared from the wild type strain, the increase in mEPSC amplitudes in Rab3A$^{-/-}$ neurons after
279 activity blockade was dramatically reduced, and the average mEPSC amplitude was not
280 significantly increased, for 25 untreated cells and 26 TTX-treated cells (Figure 1F, 13.6 ± 0.1 vs.
281 14.3 ± 0.6, $p = 0.318$, Kruskal-Wallis test). To further examine homeostatic plasticity in the
282 presence and absence of Rab3A, we computed 30 quantiles for the mEPSC amplitude
283 distribution of each neuron (Hanes et al., 2020), pooled the quantiles, and plotted the data as
284 cumulative distribution functions (CDFs) for CON and TTX. For mEPSC amplitudes from cultures
285 prepared from Rab3A$^{+/+}$ mice, the difference between CDFs was highly significant (Figure 1Gi,
286 test statistic $D = 0.172$, $p = 1.62 * 10^{-10}$, Kolmogorov Smirnov (KS) test). In contrast, the increase

287 in mEPSC amplitude after activity blockade was dramatically reduced in cortical cultures from
288 Rab3A$^{-/-}$ mice (Figure 1Hi). A KS test for the CDFs was significant, but the test statistic much
289 smaller (0.070) and the p value much larger (0.042) than for the wild type strain.

290 It was originally proposed that loss of activity produced a uniform multiplicative
291 increase in mEPSC amplitude across the entire distribution of mEPSCs (Turrigiano et al., 1998).
292 This uniform scaling would be expected to preserve original differences in synaptic weights
293 resulting from other forms of plasticity (Turrigiano, 1999; Turrigiano and Nelson, 2004). In
294 addition, uniform scaling suggested a cell-wide mechanism (in fact, a culture-wide mechanism)
295 to identically modify all synapses. However, we recently showed that in mouse cortical
296 neurons, rat cortical neurons, and mouse hippocampal neurons, scaling is non-uniform, a
297 phenomenon we called "divergent scaling;" the multiplicative factor is smallest (close to 1) for
298 small mEPSC amplitudes and increases to ~1.4 for larger mEPSC amplitudes (Hanes et al., 2020).
299 In subsequent reviewing of the current literature (Koesters et al., 2022), we concluded that the
300 majority of previous studies of homeostatic plasticity of mEPSC amplitude following activity
301 blockade also show divergent scaling, most notably the study that originally defined synaptic
302 scaling (Turrigiano et al., 1998). Divergent scaling is not obvious on the standard plot used to
303 demonstrate synaptic scaling, the rank-order plot (Turrigiano et al., 1998), but is only apparent
304 once the ratio of TTX mEPSC amplitude/CON mEPSC amplitude is computed and plotted as a
305 function of CON mEPSC amplitude (Hanes et al., 2020). To compare between uniform and
306 divergent scaling in the presence and absence of Rab3A, we created both rank order plots and
307 ratio plots for Rab3A$^{+/+}$ data. The rank order plot for Rab3A$^{+/+}$ neurons (Figure 1Gii) shows that
308 treatment with TTX appears to cause a uniform multiplication of control mEPSC amplitudes

309 based on the linear fit to the data, which had a slope of 1.43 (R^2 = 0.982). However, in the ratio
310 plot for mEPSCs in Rab3A$^{+/+}$ cultures, the scaling was clearly divergent with the smallest mEPSC
311 amplitudes having the smallest ratios (at 1) and the ratio increasing with mEPSC amplitude to a
312 maximum of 1.51 (Figure 1Giii). In the absence of Rab3A, the rank ordered mEPSC data follow
313 the line of identity and the slope of the linear fit was 0.97 (R^2 = 0.985), suggesting complete
314 absence of homeostatic plasticity (Figure 1Hii). However, the more sensitive ratio plot reveals a
315 residual divergent scaling to a peak ratio of 1.13 (Figure 1Hiii). We previously observed a
316 residual homeostatic effect of activity blockade on mEPCs at the mouse NMJ in the absence of
317 Rab3A (Wang et al., 2011) suggesting that there may be compensatory or redundant
318 mechanisms after deletion of Rab3A.

319 We next examined whether expression of a single point mutant of Rab3A (Rab3A$^{Ebd/Ebd}$)
320 would abolish synaptic scaling in the mouse cortical cultures as we previously showed for
321 mEPCs at the mouse NMJ (Wang et al., 2011). Example current traces of mEPSCs, average
322 mEPSC waveforms, and box and whisker plots are shown in Figures 2A and B, respectively, for
323 cortical cultures prepared from wild type mice in the Rab3A$^{+/Ebd}$ colony. Treatment with TTX for
324 48 hours leads to a significant increase in the average mEPSC amplitude of 23 TTX-treated cells
325 when compared to 20 untreated cells (Figure 2C, CON, 11.0 ± 0.6 pA; TTX, 15.0 ± 1.3 pA, p =
326 0.02, Kruskal-Wallis test). We note here that while the two strains respond very similarly to
327 activity blockade, the mean mEPSC amplitude in untreated cultures was significantly different in
328 the two wild type strains, 13.9 ± 0.7 pA, wild type from Rab3A$^{+/-}$ colony; 11.0 ± 0.6 pA, wild type
329 from Rab3A$^{+/Ebd}$ colony (p = 0.004, Kruskal-Wallis test).

330 We found a complete disruption of homeostatic plasticity in cortical cultures prepared
331 from Rab3A$^{Ebd/Ebd}$ mice, as can been seen in viewing example mEPSC traces and average mEPSC
332 waveforms (Figures 2D and E, respectively). The lack of TTX effect was confirmed in a
333 comparison of mEPSC amplitude means for 21 untreated and 22 TTX-treated cells (Figure 2F,
334 CON, 15.1 ± 1.0 pA vs. TTX, 14.6 ± 1.1 pA, $p = 0.81$, Kruskal-Wallis test). For cultures prepared
335 from the wild type strain of the Earlybird heterozygote colony, the CDFs of the pooled quantiles
336 from control and TTX-treated cells were significantly different (Figure 2Gi, $D = 0.177$, p value =
337 $2.88 * 10^{-9}$, KS test), but for cultures prepared from Rab3A$^{Ebd/Ebd}$ mice, the CDF of mEPSC
338 amplitudes from TTX treated cells was shifted to the *left*, indicating a slight *reduction* after
339 activity blockade, which did not reach statistical significance (Figure 2Hi; $D = 0.067$, $p = 0.097$,
340 KS test). The rank ordered data indicate that the increased slope after TTX observed in the
341 wildtype data (Figure 2Gii, slope 1.73, $R^2 = 0.993$) was completely abolished in the Earlybird
342 data (Figure 2Hii, slope 1.03, $R^2 = 0.989$). Finally, in the wild type data, the ratio of TTX mEPSC
343 amplitude/CON mEPSC amplitude increases from 1.08 for the smallest amplitudes to over 1.60
344 for the largest amplitudes (Figure 2Giii), whereas for mEPSC amplitudes from Rab3A$^{Ebd/Ebd}$
345 cultures, the ratio of TTX/CON actually falls below 1 (minimum 0.9, Figure 2 Hiii).
346 Our results show that the homeostatic increase of mEPSC amplitude after activity
347 blockade is disrupted in both Rab3A$^{-/-}$ and the Rab3A$^{Ebd/Ebd}$ cortical neurons, strongly supporting
348 a crucial role of functioning Rab3A in the synaptic scaling process. However, it is important to
349 note that the disruption differs for Rab3A$^{-/-}$ and Rab3A$^{Ebd/Ebd}$. In the Rab3A$^{-/-}$ data set, mEPSCs
350 from untreated cultures were indistinguishable from mEPSCs from Rab3A$^{+/+}$ untreated cultures,
351 demonstrating loss of Rab3A has no impact on basal activity mEPSC amplitudes, but the

352 increase in mEPSC amplitudes after activity blockade was strongly diminished in Rab3A$^{-/-}$
353 neurons. In the Rab3A$^{Ebd/Ebd}$ data set, mEPSC amplitudes from untreated cultures were
354 significantly larger than those of untreated cultures from wild type mice, as can be seen in
355 Figure 3 for the CDFs (Figure 3A, D = 0.245; p = 1.52 * 10^{-16}, KS test) and the box and whisker
356 plot (Figure 3A Inset, Rab3A$^{+/+}$, 11.0 ± 0.7 pA, vs. Rab3A$^{Ebd/Ebd}$, 15.1 ± 1.0 pA p = 0.0027). The
357 linear fit of the rank ordered data of Rab3A$^{Ebd/Ebd}$ vs. wildtype mEPSCs had a slope of 1.63
358 (Figure 3B). In the ratio plot (Figure 3C), scaling was more uniform than in any other data set we
359 have examined so far, with values starting at 1.4, declining to 1.2, then rising again to 1.4 for
360 the majority of the data, instead of beginning near 1 and rising to 1.5, as happened for
361 homeostatic plasticity (Figure 1Giii). Given this distinct behavior, it cannot be stated that the
362 presence of mutated Rab3A causes the identical effect on mEPSC amplitudes as that of activity
363 blockade. It may be that the much longer time in the presence of the Rab3A Earlybird mutant
364 compared to the 48 hour TTX treatment leads to a stable increase in the smallest mEPSCs.
365 Alternatively, these are two distinct mechanisms of mEPSC amplitude augmentation that
366 occlude each other. In any case, the increase in mEPSC amplitude in cultures from Rab3A$^{Ebd/Ebd}$
367 mice is consistent with the increase in mEPC amplitude we observed at the Rab3A$^{Ebd/Ebd}$ NMJ
368 (Wang et al., 2011).
369 The small GTPase Rab3A is generally thought to function presynaptically to regulate
370 synaptic vesicle trafficking, possibly in an activity-dependent manner (Castillo et al., 1997;
371 Lonart et al., 1998; Leenders et al., 2001; Schluter et al., 2006; Coleman and Bykhovskaia, 2009;
372 Tian et al., 2012). In contrast, homeostatic plasticity of mEPSC amplitude has been attributed to
373 an increase in postsynaptic receptors on the surface of the dendrite (O'Brien et al., 1998;

374 Turrigiano et al., 1998). Is Rab3A required for the increase in surface AMPA-type glutamate
375 receptors that has been confirmed by multiple studies (see Introduction)? It should be noted
376 that at the NMJ in vivo we could find no evidence for an increase in AChRs after TTX block of
377 the sciatic nerve in vivo (Wang et al., 2005). The type of AMPA receptor that has been shown to
378 be increased, calcium-permeable GluA1-containing AMPA receptor or calcium-impermeable
379 GluA2-containing AMPA receptor, appears to depend on the experimental manipulation. For
380 example, block of activity by APV (NMDA antagonist) combined with TTX (inhibitor of Na
381 channels) induces an increase in mEPSC amplitude in dissociated hippocampal cultures that is
382 completely reversed by acute application of the Ca-permeable receptor-specific inhibitor
383 NASPM (Sutton et al., 2006), indicating the entirety of the homeostatic effect is due to those
384 receptors, likely GluA1. In contrast, the increase in mEPSC amplitude in mouse hippocampal
385 slice cultures induced by TTX alone was not affected by another GluA1-specific inhibitor,
386 philanthotoxin, suggesting mediation by either Ca-impermeable receptors or a presynaptic
387 effect on quantal size (Soden and Chen, 2010); see also, (Dubes et al., 2022). Because we used
388 TTX alone to block network activity, we expected that NASPM would not reverse the TTX-
389 induced increase in mEPSC amplitude in our mouse cortical cultures, and we found that this
390 was indeed the case. Figure 4A shows that the TTX-induced increase in mean mEPSC amplitude
391 was nearly identical in a set of 11 CON and 11 TTX-treated cells before and after NASPM
392 treatment (before NASPM, CON 12.9 ± 3.5 pA; TTX, 17.5 ± 3.1 pA, $p = 0.009$; after NASPM, CON
393 11.9 ± 2.6 pA; TTX 16.1 ± 3.5 pA, $p = 0.006$, Kruskal-Wallis test). Application of NASPM caused a
394 modest decrease in mEPSC amplitude in both untreated and TTX-treated cultures (Figure 4B,
395 CON, before NASPM, 12.9 ± 3.5 pA; after, 11.9 ± 2.6 pA, $p = 0.08$; TTX, before NASPM, 17.5 ± 3.1

396 pA; after, 16.1 ± 3.5 pA, p = 0.08, paired t test), and also decreased mEPSC frequency (Figure
397 4C, CON, before NASPM, 1.84 sec^{-1}; after NASPM, 1.56 sec^{-1}; p = 0.003, paired t-test; TTX,
398 before NASPM, 4.40 ± 3.51 mEPSCs sec^{-1}; after NASPM, 2.68 ± 2.25 mEPSCs sec^{-1}, p = 0.02,
399 paired t-test), indicating that effective concentrations of NASPM were reached and mEPSCs due
400 to AMPA receptors composed entirely of Ca-permeable subunits were abolished.

401 Having established that GluA1 receptors are not contributing to the homeostatic
402 increase in mEPSC amplitude, we turned to immunohistochemistry and confocal imaging to
403 assess whether GluA2 receptor expression was increased in our wild type mouse cortical
404 cultures following 48 hour treatment with TTX. Since mEPSCs necessarily report synaptic levels
405 of receptors, we used VGLUT1-positivity to identify synapses on pyramidal primary apical
406 dendrites labeled with MAP-2 immunofluorescence. Figure 5 shows 6 pairs of VGLUT1- and
407 GluA2-immunofluorescent clusters (white frames) along each of two primary dendrites, one in
408 an untreated cortical culture (CON, left), the other in a culture treated with TTX for 48 hours
409 (TTX, right), both from $Rab3A^{+/+}$ mice. A dendrite typically required ~10 confocal sections to be
410 fully captured, and the total number of synaptic pairs for all the sections imaged on a dendrite
411 was usually < 20, so this is an atypically high number of pairs within a single section; these
412 particular dendrites and sections were selected for illustration purposes. In addition to the
413 synaptic pairs, we observed many GluA2-immunoreactive clusters not associated with VGLUT1
414 immunoreactivity; those along the dendrites may be extrasynaptic receptors, and those outside
415 the dendrites may be on astrocytes (Fan et al., 1999). There are also GluA2 immunoreactive
416 clusters that are close to VGLUT1 immunoreactivity but are not located along any apparent
417 MAP2-positive neurite, suggesting axon-axonal contacts, although VGLUT1 has also been

418 detected in astrocytes (Ormel et al., 2012). Only sites that contained both VGLUT1 and GluA2
419 immunoreactivity close to the primary MAP2-postive dendrite or a secondary branch were
420 selected for analyses.

421 Variability in the magnitude of the homeostatic response from culture to culture is
422 averaged out in physiological experiments by the pooling of data from many cells across many
423 cultures. To reduce the necessity for many cultures, we chose to pair experiments in the same
424 cultures by recording mEPSCs from one set of coverslips, and processing another set of
425 coverslips from the same culture for immunohistochemistry. We completed this matched
426 paradigm of physiology and immunohistochemistry, which to our knowledge has never been
427 done before, for 3 cultures prepared from Rab3A$^{+/+}$ mice and 3 cultures prepared from Rab3A$^{-/-}$
428 mice. We present the results for mEPSC data and imaging data pooled across the 3 experiments
429 in Figure 6 (Rab3A$^{+/+}$), Figure 7 (Rab3A$^{-/-}$), and Table 1. Levels of GluA2 immunoreactivity at
430 synaptic sites were quantified by the size of the GluA2-positive receptor cluster and the average
431 intensity value of the receptor cluster. We analyzed the imaging data the same way we
432 analyzed mEPSC data, sampling 30 quantiles from each dendrite's data set, and calculating the
433 means, pooling quantiles across dendrites to create CDFs, and sorting quantiles from smallest
434 to largest to produce rank order and ratio plots.

435 In the data pooled from the 3 matched experiments, neurons from Rab3A$^{+/+}$ cultures
436 showed a significant increase in mean mEPSC amplitudes following activity blockade (Figure 6A
437 inset, CON, 13.7 ± 4.5 pA, n = 23; TTX, 16.4 ± 4.3 pA, n = 24; p = 0.016, Kruskal-Wallis test); a
438 significant shift of the TTX CDF to larger mEPSC amplitude values (Figure 6A, D = 0.162, p = 1.42
439 * 10^{-8}, KS test); a slope of 1.11 in the rank order plot (Figure 6B, R^2 = 0.98); and a mean ratio of

440 the 50th to 75th percentile of 1.24 in the ratio plot (Figure 6C). These data indicate that the
441 homeostatic response averaged across the 3 cultures was very similar to, but slightly smaller
442 than, that of the previous data set presented in Figure 1. The means for size and intensity of
443 GluA2 receptor clusters, while showing trends to higher values after activity blockade, were not
444 significantly different (Figure 6D inset, size, CON, 0.97 ± 0.38 μm^2; TTX, 1.15 ± 0.59 μm^2, p =
445 0.44; Figure 6G inset, intensity, CON, 673 ± 90, TTX, 687 ± 72, p = 0.25, Kruskal-Wallis test; Table
446 1). However, when comparing the CDFs, where the sample size is much greater (equal to
447 usually close to 30 quantiles * number of cells), the shifts to larger values for the TTX CDF did
448 reach statistical significance for GluA2 receptor cluster size (Figure 6D, D = 0.089, p = 0.002, KS
449 test) and intensity (Figure 6G, D = 0.120, p = 6.73 * 10^{-6}, KS test). In the rank order plot for
450 GluA2 receptor cluster sizes (Figure 6E), the slope was actually larger than that for mEPSC
451 amplitude (1.33), but for intensity (Figure 6H), the slope value was below 1 (0.90). The weaker
452 effects on synaptic GluA2 receptor levels relative to mEPSC amplitude suggest the possibility
453 that GluA2 receptors are not the sole determining factor in the increased mEPSC amplitude
454 following activity blockade. In addition, the plot of the ratio of TTX GluA2 receptor cluster
455 size/control size as a function of ranked control values showed a surprising deviation from the
456 divergent scaling we have observed for mEPSC amplitude (compare Figure 6C to Figure 6F). The
457 smallest GluA2 receptor clusters showed a TTX/CON ratio as high as 3, but the mean ratio
458 across the 50th to 75th percentile settled down to 1.11 within < 20 samples. This finding of larger
459 ratios for the smallest GluA2 receptor clusters is supported by a previous study that followed
460 the same fluorescently labeled postsynaptic sites over time following activity blockade. Wang
461 and colleagues found that the biggest increases after activity blockade occurred at the

462 smallest/dimmest synaptic sites (Wang et al., 2019). A similar inverse relationship was reported
463 for changes in individual fluorescently labeled postsynaptic sites followed over time under
464 normal activity conditions (Minerbi et al., 2009; Statman et al., 2014). The mismatch in ratio
465 values between the smallest mEPSC amplitudes and smallest GluA2 receptor cluster sizes may
466 be due to the inability of physiological assays to detect the mEPSCs coming from the smallest
467 synapses.

468 We proceeded to determine the homeostatic responses of mEPSC amplitude and GluA2
469 receptor levels in 3 cultures prepared from Rab3A$^{-/-}$ mice. As shown for the data set in Figure 1,
470 mean mEPSC amplitude was not increased following activity blockade in the data pooled from
471 this new set of 3 Rab3A$^{-/-}$ cultures (Figure 7A inset, CON 14.9 ± 3.8 pA, n = 21; TTX, 14.0 ± 4.0
472 pA, n = 19; p = 0.34, Kruskal-Wallis test). Notably, the TTX CDF was shifted to *smaller* mEPSC
473 amplitude values (Figure 7A, D = 0.072, p = 0.085, KS test), the slope of the rank order plot was
474 below 1 (Figure 7B, slope 0.93, R^2 = 0.997), and the mean ratio across the 50th to 75th percentile
475 was below 1 (Figure 7C, 0.96). Thus, the disruption of homeostatic plasticity of mEPSC
476 amplitude shown with the previous data sets was recapitulated in this data set. For
477 immunohistochemistry results from the same Rab3A$^{-/-}$ cultures, we found that mean GluA2
478 receptor cluster size was unchanged following activity blockade (Figure 7D inset, CON, 0.93 ±
479 0.27 μm^2, TTX, 0.91 ± 0.28 μm^2, p = 0.74, Kruskal-Wallis test), the TTX CDF was not significantly
480 shifted (Figure 7D, D = 0.045, p = 0.31, KS test), the slope on the rank order plot was 1.01
481 (Figure 7E), and the ratio hovered at or below 1 except for a small group of ratios at the high
482 end of the control values (Figure 7F). For intensity, mean values were not increased after
483 activity blockade (Figure 7G inset, CON, 766 ± 68, TTX, 776 ± 79, p = 0.47, Kruskal-Wallis test),

484 the CDFs were not significantly different (Figure 7G, D = 0.060, p = 0.080), the slope on the rank
485 order plot was 1.09 (Figure 7H), and the mean ratio value across the 50th to 75th percentile was
486 1.02 (Figure 7I). Taken together, these results indicate that the modest increases in GluA2
487 receptor cluster size and intensity following activity blockade observed in wild-type cultures do
488 not occur in the absence of Rab3A.

489 As noted above, the magnitude of the homeostatic effect on mEPSC amplitude
490 appeared to be more robust than that on receptor levels in cultures from $Rab3A^{+/+}$ mice.
491 Further evidence that there is not a one-to-one correspondence in the homeostatic response of
492 mEPSC amplitudes and GluA2 receptor levels was apparent when the individual experiments'
493 data were compared. The electrophysiology experiments were technically difficult because in
494 order to evaluate whether a particular culture displayed homeostatic plasticity of mEPSC
495 amplitude, we set a minimum requirement of recording from 6 cells per condition, meaning a
496 successful experiment required at least 12 (6 CON and 6 TTX) usable recordings (i.e. low holding
497 current, stable baseline, low noise, etc.) in one day. Ultimately, our sample size ranged from 6
498 to 10 cells per condition per culture. Figures 8A-C show the CDFs and ratio plots for 3 individual
499 $Rab3A^{+/+}$ cultures. Rank order plots are not included here because the ratio plot is more
500 sensitive than the rank order plot when determining effect magnitude. We found that the
501 mEPSC amplitude effects differed from the GluA2 cluster size effects at both the broad level
502 (increases vs decreases), and in the specific ways in which the effect was non-uniform. Broadly,
503 although two of the three $Rab3A^{+/+}$ experiments show a homeostatic increase in the TTX CDF
504 and a ratio of TTX/CON > 1 for both mEPSC amplitudes (Figures 8Ai,iii and 8Bi,iii) and synaptic
505 GluA2 receptor cluster sizes (Figures 8Aii,iv and 8Bii,iv), Culture #3 shows an increase in mEPSC

506 amplitude but a *decrease* in the GluA2 receptor cluster size, based on both the shifts in CDFs
507 (mEPSC, Figure 8Ci, vs GluA2 receptor cluster size, Figure 8Cii) and the majority of ratio values
508 (mEPSC, Figure 8Ciii, vs. GluA2 receptor cluster size, Figure 8Civ). Similarly, we found an obvious
509 mismatch between the mEPSC amplitude data and the GluA2 cluster size data for one of the
510 three Rab3A$^{-/-}$ experiments. For Culture #3, the mEPSC TTX CDF shows a shift to the left (Figure
511 8Fi), and the ratios were below 1 for control mEPSC amplitudes < 20 pA and above 1 for control
512 mEPSC amplitudes > 20 pA (Figure 8Fiii). In the same culture, GluA2 receptor cluster size CDF
513 shows a shift to the right after activity blockade (Figure 8Fii), and in the ratio plot, values were
514 at or above 1 throughout the range of control sizes (Figure 8Fiv).

515 Perhaps more striking than the broad mismatches, which could be attributed to the
516 small sample sizes, is the complete lack of correspondence of TTX/CON ratios in the mEPSC
517 amplitudes compared to GluA2 cluster sizes in the same cultures. In cultures from Rab3A$^{+/+}$
518 mice, mEPSC amplitudes show divergent scaling similar to what we have previously reported,
519 with the smallest CON amplitudes showing the smallest ratios, and the ratio increasing
520 monotonically to a plateau, or, a peak followed by a gradual decline, as CON mEPSC amplitude
521 becomes very large. In contrast, the very smallest GluA2 cluster sizes in Rab3A$^{+/+}$ cultures have
522 the largest increase, with ratios as high as 3 in the two cultures that showed a broad overall
523 increase. The ratios decline dramatically to values around 1.5, but then remain substantially
524 above 1 throughout the entire range of data. Interestingly, the dramatic increase in the size of
525 the smallest GluA2 clusters is absent in the two cultures from Rab3A$^{-/-}$ mice that broadly
526 showed no increase, suggesting this aspect is also dependent on Rab3A. It is not even possible
527 to cut off the ratios at a certain point, to address a threshold effect such as GluA2 cluster sizes

528 below a certain value not being measurable electrophysiologically, and get the ratios for the
529 remaining data to match up. Taken together, these data indicate that variation in homeostatic
530 effects on GluA2 cluster size is not responsible for the variation in homeostatic effects on
531 mEPSC amplitude.

532 In summary, our matched mEPSC and receptor cluster results indicate that: 1. activity
533 blockade resulted in an increase in mEPSC amplitudes and synaptic GluA2 receptors; 2. loss of
534 Rab3A disrupted both the increase in mEPSC amplitudes and the increase in GluA2 receptor
535 levels; and 3. The homeostatic effects on mEPSC amplitudes and the GluA2 cluster sizes within
536 the same cultures differed at both the broad level, and in the specific way the ratios were non-
537 uniform, making it difficult to conclude modulation of GluA2 cluster size is the sole determinant
538 of homeostatic increases in mEPSC amplitude. Although it remains a possibility that the
539 disparities in homeostatic effects on mEPSC amplitudes and GluA2 cluster size TTX/CON ratios
540 might arise due to a sampling error, given the small number of cells sampled in each individual
541 experiment ($\leq$ 10), it seems unlikely that differences arising from sampling error alone would be
542 so consistent. However, only when we are able to more easily sample larger numbers of cells,
543 or it becomes possible to measure mEPSCs and receptor levels in the same cells, will we be able
544 to resolve this question.

545 We have demonstrated here for the first time that the synaptic vesicle protein Rab3A
546 influences the homeostatic regulation of postsynaptic GluA2 receptors. What are possible ways
547 that Rab3A could exert a postsynaptic action? It has previously been shown that exogenous
548 addition of TNFα to hippocampal cultures causes an increase in surface expression of GluA1
549 receptors (although not GluA2 receptors), and that the homeostatic increase in mEPSC

550 amplitudes is abolished in cultures prepared from the TNFα deletion mouse (Stellwagen et al.,
551 2005; Stellwagen and Malenka, 2006). Furthermore, neurons from TNF$\alpha^{+/+}$ mice plated on
552 astrocytic feeder layers derived from TNF$\alpha^{-/-}$ mice fail to show the increase in mEPSC amplitude
553 after TTX treatment, indicating that the TNFα inducing the receptor increases following activity
554 blockade comes from the astrocytes (Stellwagen and Malenka, 2006). Rab3A has been detected
555 in astrocytes (Maienschein et al., 1999; Hong et al., 2016), so to determine whether Rab3A is
556 acting via regulating TNFα release from astrocytes, we performed experiments similar to those
557 of Stellwagen and Malenka (2006) (schema illustrated in Figure 9, left side). We compared the
558 effect of activity blockade on mEPSC amplitudes recorded from cortical neurons from Rab3A$^{+/+}$
559 mice plated on Rab3A$^{+/+}$ astrocytic feeder layers (Figure 9A); neurons from Rab3A$^{+/+}$ mice
560 plated on Rab3A$^{-/-}$ astrocytes (Figure 9B), and neurons from Rab3A$^{-/-}$ mice plated on Rab3A$^{+/+}$
561 astrocytes (Figure 9C). If Rab3A is required for TNFα release from astrocytes, then Rab3A$^{+/+}$
562 neurons plated on Rab3A$^{-/-}$ astrocytes should not show a homeostatic increase in mEPSC
563 amplitude after treatment with TTX, and any cultures with Rab3A$^{+/+}$ astrocytes should have a
564 normal homeostatic response. We found the opposite result: mEPSC amplitudes increased
565 dramatically in cultures where Rab3A was present in neurons (Figures 9A and B), but much
566 more modestly increased in cultures where Rab3A was present only in astrocytes (Figure 9C).
567 Interestingly, the homeostatic effects appear to be larger in the feeder layer cultures,
568 compared to the effects observed in our previous neuronal/astrocyte mixed cultures prepared
569 directly onto poly-L-lysine coated coverslips, but the ratio plots clearly show scaling was
570 divergent under both plating conditions (compare Figures 1Giii with Figures 9Aiii and Biii). We
571 noticed that in the astrocyte feeder layer cultures, and in the matched mEPSC amplitude and

572 GluA2 receptor measurement experiments, the mean mEPSC amplitude in the untreated
573 cultures prepared from Rab3A$^{-/-}$ mice was slightly, but not significantly, larger, compared to the
574 mean mEPSC amplitude for untreated cultures prepared from Rab3A$^{+/+}$ mice in the same
575 experiments (astrocyte feeder layer, Rab3A$^{+/+}$ neurons on Rab2A$^{+/+}$ astrocytes, 13.3 ± 0.5 pA,
576 Rab3A$^{-/-}$ on Rab3A$^{+/+}$ astrocytes, 15.2 ± 1.1 pA; matched mEPSC and receptor experiments,
577 Rab3A$^{+/+}$ 13.7 ± 4.5 pA, Rab3A$^{-/-}$ 14.9 ± 3.8 pA. It is therefore possible that loss of Rab3A, like
578 expression of the Rab3A Earlybird mutant, affects basal mEPSC amplitude, albeit to a lesser
579 extent. However, it could also be that these differences reflect random variation in mEPSC
580 amplitude from culture to culture.

581 In summary, in the absence of Rab3A from astrocytes, the divergent scaling of mEPSC
582 amplitude following activity blockade was completely normal, whereas in the absence of Rab3A
583 in neurons, scaling was greatly diminished. This result makes it highly unlikely that Rab3A is
584 required for the release of TNFα, or another factor from astrocytes, that induces a homeostatic
585 upregulation of postsynaptic receptors and thereby increases mEPSC amplitude following TTX
586 treatment. Neuronal Rab3A appears to mediate the homeostatic increase in mEPSC amplitude
587 following activity blockade.

588

589 <u>Discussion</u>

590 We found that homeostatic synaptic plasticity of mEPSC amplitude in dissociated mixed
591 cultures of mouse cortical neurons and astrocytes behaved remarkably similar to the mouse
592 NMJ in response to loss of Rab3A function: scaling up of mEPSC amplitude following prolonged

593 network silencing by TTX was strongly diminished in cultures from Rab3A$^{-/-}$, and in cultures
594 from Rab3A$^{Ebd/Ebd}$ mice, basal mEPSC amplitude was increased compared to that of wild-type
595 cultures and was not further modified following 48-hour treatment with TTX. These results
596 suggest that normal function of the presynaptic vesicle protein Rab3A is required for the
597 homeostatic scaling up of mEPSC amplitude in cortical cultures and at the NMJ in vivo.

598

599 *Rab3A not likely to regulate receptor trafficking*

600 We demonstrated that an increase in synaptic GluA2 receptors accompanies the
601 increase in mEPSC amplitude in cultures of dissociated mouse cortical neurons after 48-hour
602 TTX treatment. By examining the same cultures with both mEPSC and immunofluorescence
603 measurements, we found: 1. the effect on GluA2 receptor levels, whether measured as the size
604 of a synaptic cluster or the density of receptors in a cluster, was less robust than the effect on
605 mEPSC amplitudes; 2. the homeostatic effect on mEPSC amplitudes and GluA2 receptors
606 substantially differed from each other both broadly (mEPSC amplitudes could increase while
607 GluA2 cluster sizes decreased, and vice versa), and in the details of non-uniform scaling, one
608 example being that the smallest mEPSC amplitudes showed the least effects but the smallest
609 GluA2 clusters showed the greatest effects. Interestingly, there are other examples where the
610 effect of activity blockade by either TTX alone (Hu et al., 2010), TTX and AP5 (Letellier et al.,
611 2014), or DNQX (Blackman et al., 2012) on AMPAR levels did not match that of mEPSC
612 amplitudes, although in these cases, the increases in receptors were larger than the increases
613 of mEPSC amplitudes. The striking differences between TTX effects on AMPARs and mEPSC

614 amplitudes indicates that there may be another factor contributing to mEPSC amplitude
615 besides levels of AMPAR expression. One possibility is alterations in the type of AMPA receptor
616 expressed, since GluA1 homomers have much greater conductance than GluA2-containing
617 receptors (Oh and Derkach, 2005; Benke and Traynelis, 2019). Increases in mEPSC amplitudes
618 not accompanied by increases in receptor numbers have been attributed to such a switch (Hou
619 et al., 2015; Silva et al., 2019; Dubes et al., 2022).

620 In addition to finding a disparity between synaptic GluA2 receptor and mEPSC responses
621 to prolonged activity blockade, there are two other reasons we do not think Rab3A impacts
622 homeostatic synaptic plasticity solely through postsynaptic regulation of GluA2 receptor
623 trafficking to the plasma membrane. First, prolonged activity blockade with TTX at the NMJ led
624 to an increase in mEPC amplitude that was not accompanied by an increase in AChR levels, yet
625 it was dependent on Rab3A (Wang et al., 2011). Second, for Rab3A to modulate AMPAR
626 trafficking, it must be located in the postsynaptic dendrite. Multiple presynaptic molecules,
627 such as SNARE proteins, synaptotagmins, and NSF have been identified in the postsynaptic
628 compartment (Lledo et al., 1998; Nishimune et al., 1998; Osten et al., 1998; Song et al., 1998;
629 Araki et al., 2010; Kennedy et al., 2010; Suh et al., 2010; Jurado et al., 2013; Hussain and
630 Davanger, 2015; Gu et al., 2016; Wu et al., 2017), but to our knowledge, Rab3A has not.
631

632 *Rab3A may regulate quantal size presynaptically*

633 Based on our findings, the lack of postsynaptic Rab3A expression and the known
634 presynaptic expression of Rab3A, Rab3A may regulate mEPSC amplitude presynaptically by
635 modulating: a) the amount of transmitter transported into the vesicle, b) the size of the vesicle,

636 or c) fusion pore characteristics. mRNA for the glutamate transporter, VGLUT1, was increased in
637 rat cortical cultures after 48-hr treatment with TTX (De Gois et al., 2005), and VGLUT1 relative
638 to synapsin I in rat hippocampal cultures was increased after 48-hr treatment with AP-5 (Wilson
639 et al., 2005). This activity-dependent regulation of VGLUT1 was recently corroborated in a
640 proteome study (Dorrbaum et al., 2020), and it has also been shown that mEPSC amplitudes are
641 increased after overexpression of VGLUT at the Drosophila NMJ (Daniels et al., 2004) and in rat
642 hippocampal cultures (Wilson et al., 2005). These data suggest that increases in VGLUT1 after
643 activity-blockade could contribute to the homeostatic increase in mEPSC amplitude. Although
644 there is no direct evidence for an interaction between VGLUT1 and Rab3A, Rab3A levels are
645 reduced 50% in hippocampal extracts from mice lacking VGLUT1 (Fremeau et al., 2004). A
646 Rab3A-dependent modulation of presynaptic quantal size would explain the homeostatic
647 effects on mEPSC amplitudes that are not matched by changes in receptor levels.

648 Interestingly, Rab3A plays a role in regulating vesicle size. In adrenal chromaffin cells
649 from mice lacking all 4 Rab3 isoforms (A, B, C and D) or mice heterozygous for Rab3A and
650 lacking the B, C, and D isoforms ($Rab3A^{+/-}BCD^{-/-}$) with only 1 copy of Rab3A, there was a 20%
651 increase in large dense core vesicle (DCV) diameter that did not reach significance ($p = 0.11$)
652 (Schonn et al., 2010). Similarly, in the exocrine pancreas and parotid gland of the $Rab3D^{-/-}$, large
653 DCV diameter was increased by 22% (Riedel et al., 2002). This magnitude of change in diameter
654 would produce a greater than 80% increase in volume. Also, an increase in volume has been
655 shown to increase miniature endplate junctional current amplitude at the Drosophila NMJ
656 (Karunanithi et al., 2002). There have not been any reports that small synaptic vesicle size is
657 increased in $Rab3^{-/-}$mice, but small synaptic vesicle size is regulated by activity: vesicle size

658 increased in retinotectal terminals within the optic tectum following enucleation in pigeon
659 (Cuenod et al., 1970), with similar results in cat and monkey (Lloret and Saavedra, 1975), in rat
660 caudate nucleus following cortical ablation (Kawana et al., 1971), and in rat ventral spinal cord
661 following immobilization (Cheresharov et al., 1978).

662 Finally, we previously showed that at the mouse NMJ, both loss of Rab3A and activity
663 blockade by TTX caused an increase in the frequency of abnormally slow rising and/or
664 prolonged duration mEPCs (Wang et al., 2011). We further demonstrated that the loss of Rab3A
665 increased the frequency of very small amplitude fusion pore feet in mouse chromaffin cells
666 (Wang et al., 2008). Taken together, these data suggested that Rab3A acts to prevent abnormal
667 fusion pore release events. However, at the NMJ and in chromaffin cells, the kinetics (rise time,
668 decay, half width) of the vast majority of release events were unchanged in the absence of
669 Rab3A, making it unlikely that the shift in the distribution of mEPSC amplitudes is mediated by a
670 Rab3A-dependent change in fusion pore kinetics.

671

672 *Neuronal, not astrocytic, Rab3A may be required for the homeostatic release of a signaling*
673 *molecule*

674 Our results support the surprising possibility that presynaptic Rab3A regulates
675 postsynaptic AMPARs, rather than occurring through a direct effect on the trafficking of
676 AMPARs by Rab3A in the dendrite. Astrocytic release of TNFα was shown to mediate the
677 increase in AMPARs in prolonged activity-blocked hippocampal cultures (Stellwagen and
678 Malenka, 2006), but we found that loss of Rab3A in astrocytes does not disrupt the increase in

679 mEPSC after activity blockade. Further, we previously showed that the homeostatic increase in
680 NMJ mEPC amplitude was completely normal in the absence of TNFα (Wang et al., 2011).
681 Another possible way Rab3A might mediate regulation of postsynaptic AMPARs is
682 through the presynaptic release of a signaling molecule, such as brain-derived neurotrophic
683 factor (BDNF), that acts anterogradely to alter postsynaptic AMPAR levels. Addition of
684 exogenous BDNF to neuronal cultures prevents the increase in mEPSC amplitude following
685 activity blockade (Rutherford et al., 1998; Benevento et al., 2016) but see (Smith-Dijak et al.,
686 2019), and BDNF mRNA is reduced after activity blockade in vitro (Benevento et al., 2016;
687 Miyasaka and Yamamoto, 2021) and in vivo (Castren et al., 1992). Also, after reduction of
688 secreted BDNF in culture media via the BDNF scavengers TrkB-FC or TrkB-IgG, mEPSC
689 amplitudes are increased (Rutherford et al., 1998; Benevento et al., 2016; Smith-Dijak et al.,
690 2019). Rab3B, a Rab3 family member with strong homology to Rab3A but expressed more
691 highly in inhibitory nerve terminals (Tsetsenis et al., 2011), is modified epigenetically following
692 TTX treatment by the same DNA methylation pathway as that for BDNF (Benevento et al.,
693 2016). In addition, reduction of Rab3A in astrocytes decreases astrocytic BDNF release (Hong et
694 al., 2016), and treatment of cultures with BDNF can increase Rab3A levels (Takei et al., 1997;
695 Thakker-Varia et al., 2001) but see (Shinoda et al., 2014). Taken together, these results suggest
696 an interplay between BDNF and Rab3A in the activity-dependent regulation of AMPA receptors.
697
698 *Rab3A is required for divergent scaling*
699 We have established that homeostatic synaptic plasticity in mouse cortical cultures, rat
700 cortical cultures, and mouse hippocampal cultures demonstrates divergent, rather than

701 uniform, scaling (Hanes et al., 2020; Koesters et al., 2022). The deviation from uniformity
702 suggests that individual synapses may be independently regulated, and do not require a global,
703 cell-wide signal. Our conclusion is supported by multiple studies demonstrating local activity-
704 dependent regulation of mEPSC amplitudes at subsets of synapses (Ju et al., 2004; Sutton et al.,
705 2006; Hou et al., 2008; Beique et al., 2011; Hou et al., 2011; Letellier et al., 2014). It is further
706 supported by the recent finding that in hippocampal cultures treated with TTX, AMPA receptors
707 increase selectively at synaptopodin-positive sites, which are already larger and contain higher
708 amounts of AMPA receptors (Dubes et al., 2022). The authors provide evidence that the
709 process depends on the microRNA miR-124: miR-124 is reduced after activity blockade; and
710 overexpression of miR-124 blocks the TTX-induced increase in AMPA receptors and mEPSC
711 amplitudes. Increases in miR-124 have also been linked to decreases in mEPC amplitudes at the
712 NMJs of the slow channel syndrome mouse (mSCS) in which prolongation of ACh currents
713 causes excess excitation (Zhu et al., 2013). Zhu and colleagues provide evidence for a
714 postsynaptic calpain-Cdk5-nNOS pathway that is activated by increased calcium levels, with the
715 NO feeding back retrogradely to regulate miR-124, which in turn directly interacts with Rab3A
716 to affect quantal content (Zhu et al., 2013), but it is also possible that Rab3A is contributing to
717 the mEPSC amplitude changes in mSCS. In sum, these studies suggest miR-124 could tie
718 together presynaptic changes (Rab3A, transmitter released from a single vesicle) and
719 postsynaptic changes (synaptopodin, AMPA receptors) in divergent homeostatic synaptic
720 plasticity.

721

722 *A model for the role of Rab3A in homeostatic plasticity of mEPSC amplitude*

723 We propose a model for Rab3A function in homeostatic synaptic plasticity of mEPSC
724 amplitude in which Rab3A contributes to presynaptic quantal size through the amount of
725 transmitter released by fusion of a single vesicle, and to postsynaptic quantal size through the
726 number of postsynaptic receptors. Normally, Rab3A cycles between GTP and GDP-bound forms
727 ("State 1," indicated by red tag in Figure 10A) and promotes synaptic vesicle mobilization and
728 fusion, at the same time maintaining vesicle size/transmitter content within a narrow range. In
729 this normally cycling Rab3A state, an anterograde signal dependent on Rab3A maintains GluA2
730 receptors at their normal, restricted level. Activity blockade leads to a buildup of an alternate
731 form of Rab3A, possibly one that is unable to cycle through its GTP and GDP-bound forms
732 ("State 2," indicated by gray tag in Figure 10B). Without the quality control mechanism
733 conferred by State 1 Rab3A, vesicle size/transmitter content skews to higher values, and the
734 anterograde signal is abnormal, leading to GluA2 receptors levels rising outside normal limits.
735 Not shown here, the Earlybird point mutation may permanently be in "State 2," as the mutation
736 is in the guanine nucleotide binding region (Kapfhamer), which would lead to increased
737 transmitter released from single vesicles and increased receptor levels.

738 We have demonstrated an essential role of the presynaptic vesicle protein Rab3A in the
739 homeostatic increase in mEPSC amplitude and GluA2 AMPA receptor levels at synaptic sites in
740 mouse dissociated cortical cultures. To our knowledge, this is the first evidence of a presynaptic
741 protein being implicated in the homeostatic regulation of mEPSC amplitude and AMPARs in
742 neuronal cultures. The current results extend our previous findings that showed the
743 homeostatic increase in mEPC amplitudes at the mouse NMJ in vivo depends on Rab3A. Under
744 conditions where postsynaptic receptors are close to being saturated by the amount of

745 transmitter in a single vesicle (possibly in cortical cultures but not at the NMJ), it may be
746 necessary to increase both the amount of transmitter released and the number or function of
747 postsynaptic receptors in order to observe a homeostatic increase in the physiological signal,
748 mEPSC amplitude. Our results suggest that in cortical cultures, neuronal Rab3A is a key player
749 regulating the homeostatic increase in synaptic strength on both sides of the synapse.

750

751 References

752 Altimimi HF, Stellwagen D (2013) Persistent synaptic scaling independent of AMPA receptor subunit
753 composition. J Neurosci 33:11763-11767.
754 Anggono V, Clem RL, Huganir RL (2011) PICK1 loss of function occludes homeostatic synaptic scaling. J
755 Neurosci 31:2188-2196.
756 Araki Y, Lin DT, Huganir RL (2010) Plasma membrane insertion of the AMPA receptor GluA2 subunit is
757 regulated by NSF binding and Q/R editing of the ion pore. Proc Natl Acad Sci U S A 107:11080-
758 11085.
759 Beique JC, Na Y, Kuhl D, Worley PF, Huganir RL (2011) Arc-dependent synapse-specific homeostatic
760 plasticity. Proc Natl Acad Sci U S A 108:816-821.
761 Benevento M, Iacono G, Selten M, Ba W, Oudakker A, Frega M, Keller J, Mancini R, Lewerissa E, Kleefstra
762 T, Stunnenberg HG, Zhou H, van Bokhoven H, Nadif Kasri N (2016) Histone Methylation by the
763 Kleefstra Syndrome Protein EHMT1 Mediates Homeostatic Synaptic Scaling. Neuron 91:341-355.
764 Benke T, Traynelis SF (2019) AMPA-Type Glutamate Receptor Conductance Changes and Plasticity: Still a
765 Lot of Noise. Neurochem Res 44:539-548.
766 Blackman MP, Djukic B, Nelson SB, Turrigiano GG (2012) A critical and cell-autonomous role for MeCP2
767 in synaptic scaling up. J Neurosci 32:13529-13536.
768 Castillo PE, Janz R, Sudhof TC, Tzounopoulos T, Malenka RC, Nicoll RA (1997) Rab3A is essential for
769 mossy fibre long-term potentiation in the hippocampus. Nature 388:590-593.
770 Castren E, Zafra F, Thoenen H, Lindholm D (1992) Light regulates expression of brain-derived
771 neurotrophic factor mRNA in rat visual cortex. Proc Natl Acad Sci U S A 89:9444-9448.
772 Cheresharov L, Ovtscharoff W, Manolov S (1978) Ultrastructural changes in the anterior horn synapses
773 of rat spinal cord under different locomotor conditions. J Neural Transm 42:9-21.
774 Coleman WL, Bykhovskaia M (2009) Rab3a-mediated vesicle recruitment regulates short-term plasticity
775 at the mouse diaphragm synapse. Mol Cell Neurosci 41:286-296.
776 Coleman WL, Bill CA, Bykhovskaia M (2007) Rab3a deletion reduces vesicle docking and transmitter
777 release at the mouse diaphragm synapse. Neuroscience 148:1-6.
778 Correa SA, Hunter CJ, Palygin O, Wauters SC, Martin KJ, McKenzie C, McKelvey K, Morris RG, Pankratov
779 Y, Arthur JS, Frenguelli BG (2012) MSK1 regulates homeostatic and experience-dependent
780 synaptic plasticity. J Neurosci 32:13039-13051.
781 Cuenod M, Sandri C, Akert K (1970) Enlarged synaptic vesicles as an early sign of secondary
782 degeneration in the optic nerve terminals of the pigeon. J Cell Sci 6:605-613.

783 Daniels RW, Collins CA, Gelfand MV, Dant J, Brooks ES, Krantz DE, DiAntonio A (2004) Increased
784 expression of the Drosophila vesicular glutamate transporter leads to excess glutamate release
785 and a compensatory decrease in quantal content. J Neurosci 24:10466-10474.
786 De Gois S, Schafer MK, Defamie N, Chen C, Ricci A, Weihe E, Varoqui H, Erickson JD (2005) Homeostatic
787 scaling of vesicular glutamate and GABA transporter expression in rat neocortical circuits. J
788 Neurosci 25:7121-7133.
789 Diering GH, Gustina AS, Huganir RL (2014) PKA-GluA1 coupling via AKAP5 controls AMPA receptor
790 phosphorylation and cell-surface targeting during bidirectional homeostatic plasticity. Neuron
791 84:790-805.
792 Diering GH, Nirujogi RS, Roth RH, Worley PF, Pandey A, Huganir RL (2017) Homer1a drives homeostatic
793 scaling-down of excitatory synapses during sleep. Science 355:511-515.
794 Dorrbaum AR, Alvarez-Castelao B, Nassim-Assir B, Langer JD, Schuman EM (2020) Proteome dynamics
795 during homeostatic scaling in cultured neurons. Elife 9.
796 Dubes S, Soula A, Benquet S, Tessier B, Poujol C, Favereaux A, Thoumine O, Letellier M (2022) miR-124-
797 dependent tagging of synapses by synaptopodin enables input-specific homeostatic plasticity.
798 EMBO J 41:e109012.
799 Fan D, Grooms SY, Araneda RC, Johnson AB, Dobrenis K, Kessler JA, Zukin RS (1999) AMPA receptor
800 protein expression and function in astrocytes cultured from hippocampus. J Neurosci Res
801 57:557-571.
802 Fernandes D, Carvalho AL (2016) Mechanisms of homeostatic plasticity in the excitatory synapse. J
803 Neurochem 139:973-996.
804 Fremeau RT, Jr., Kam K, Qureshi T, Johnson J, Copenhagen DR, Storm-Mathisen J, Chaudhry FA, Nicoll
805 RA, Edwards RH (2004) Vesicular glutamate transporters 1 and 2 target to functionally distinct
806 synaptic release sites. Science 304:1815-1819.
807 Gainey MA, Hurvitz-Wolff JR, Lambo ME, Turrigiano GG (2009) Synaptic scaling requires the GluR2
808 subunit of the AMPA receptor. J Neurosci 29:6479-6489.
809 Gainey MA, Tatavarty V, Nahmani M, Lin H, Turrigiano GG (2015) Activity-dependent synaptic GRIP1
810 accumulation drives synaptic scaling up in response to action potential blockade. Proc Natl Acad
811 Sci U S A 112:E3590-3599.
812 Gao M, Sossa K, Song L, Errington L, Cummings L, Hwang H, Kuhl D, Worley P, Lee HK (2010) A specific
813 requirement of Arc/Arg3.1 for visual experience-induced homeostatic synaptic plasticity in
814 mouse primary visual cortex. J Neurosci 30:7168-7178.
815 Geppert M, Bolshakov VY, Siegelbaum SA, Takei K, De Camilli P, Hammer RE, Sudhof TC (1994) The role
816 of Rab3A in neurotransmitter release. Nature 369:493-497.
817 Gu Y, Chiu SL, Liu B, Wu PH, Delannoy M, Lin DT, Wirtz D, Huganir RL (2016) Differential vesicular sorting
818 of AMPA and GABAA receptors. Proc Natl Acad Sci U S A 113:E922-931.
819 Hanes AL, Koesters AG, Fong MF, Altimimi HF, Stellwagen D, Wenner P, Engisch KL (2020) Divergent
820 Synaptic Scaling of Miniature EPSCs following Activity Blockade in Dissociated Neuronal Cultures.
821 J Neurosci 40:4090-4102.
822 Hong Y, Zhao T, Li XJ, Li S (2016) Mutant Huntingtin Impairs BDNF Release from Astrocytes by Disrupting
823 Conversion of Rab3a-GTP into Rab3a-GDP. J Neurosci 36:8790-8801.
824 Hou Q, Gilbert J, Man HY (2011) Homeostatic regulation of AMPA receptor trafficking and degradation
825 by light-controlled single-synaptic activation. Neuron 72:806-818.
826 Hou Q, Zhang D, Jarzylo L, Huganir RL, Man HY (2008) Homeostatic regulation of AMPA receptor
827 expression at single hippocampal synapses. Proc Natl Acad Sci U S A 105:775-780.
828 Hou Q, Ruan H, Gilbert J, Wang G, Ma Q, Yao WD, Man HY (2015) MicroRNA miR124 is required for the
829 expression of homeostatic synaptic plasticity. Nat Commun 6:10045.

830 Hu JH, Park JM, Park S, Xiao B, Dehoff MH, Kim S, Hayashi T, Schwarz MK, Huganir RL, Seeburg PH,
831 Linden DJ, Worley PF (2010) Homeostatic scaling requires group I mGluR activation mediated by
832 Homer1a. Neuron 68:1128-1142.
833 Hussain S, Davanger S (2015) Postsynaptic VAMP/Synaptobrevin Facilitates Differential Vesicle
834 Trafficking of GluA1 and GluA2 AMPA Receptor Subunits. PLoS One 10:e0140868.
835 Ju W, Morishita W, Tsui J, Gaietta G, Deerinck TJ, Adams SR, Garner CC, Tsien RY, Ellisman MH, Malenka
836 RC (2004) Activity-dependent regulation of dendritic synthesis and trafficking of AMPA
837 receptors. Nat Neurosci 7:244-253.
838 Jurado S, Goswami D, Zhang Y, Molina AJ, Sudhof TC, Malenka RC (2013) LTP requires a unique
839 postsynaptic SNARE fusion machinery. Neuron 77:542-558.
840 Kapfhamer D, Valladares O, Sun Y, Nolan PM, Rux JJ, Arnold SE, Veasey SC, Bucan M (2002) Mutations in
841 Rab3a alter circadian period and homeostatic response to sleep loss in the mouse. Nat Genet
842 32:290-295.
843 Karunanithi S, Marin L, Wong K, Atwood HL (2002) Quantal size and variation determined by vesicle size
844 in normal and mutant Drosophila glutamatergic synapses. J Neurosci 22:10267-10276.
845 Kavalali ET, Monteggia LM (2023) Rapid homeostatic plasticity and neuropsychiatric therapeutics.
846 Neuropsychopharmacology 48:54-60.
847 Kawana E, Akert K, Bruppacher H (1971) Enlargement of synaptic vesicles as an early sign of terminal
848 degneration in the rat caudate nucleus. J Comp Neurol 142:297-307.
849 Kennedy MJ, Davison IG, Robinson CG, Ehlers MD (2010) Syntaxin-4 defines a domain for activity-
850 dependent exocytosis in dendritic spines. Cell 141:524-535.
851 Koesters AG, Rich MM, Engisch KL (2022) Diverging from the Norm: Reevaluating What Miniature
852 Excitatory Postsynaptic Currents Tell Us about Homeostatic Synaptic Plasticity.
853 Neuroscientist:10738584221112336.
854 Leenders AG, Lopes da Silva FH, Ghijsen WE, Verhage M (2001) Rab3a is involved in transport of synaptic
855 vesicles to the active zone in mouse brain nerve terminals. Mol Biol Cell 12:3095-3102.
856 Letellier M, Elramah S, Mondin M, Soula A, Penn A, Choquet D, Landry M, Thoumine O, Favereaux A
857 (2014) miR-92a regulates expression of synaptic GluA1-containing AMPA receptors during
858 homeostatic scaling. Nat Neurosci 17:1040-1042.
859 Lignani G, Baldelli P, Marra V (2020) Homeostatic Plasticity in Epilepsy. Front Cell Neurosci 14:197.
860 Lledo PM, Zhang X, Sudhof TC, Malenka RC, Nicoll RA (1998) Postsynaptic membrane fusion and long-
861 term potentiation. Science 279:399-403.
862 Lloret IL, Saavedra JP (1975) Enlargement of synaptic vesicles in degenerating nerve endings: a
863 comparison between cat and monkey. J Neurocytol 4:1-6.
864 Lonart G, Janz R, Johnson KM, Sudhof TC (1998) Mechanism of action of rab3A in mossy fiber LTP.
865 Neuron 21:1141-1150.
866 Lovinger DM, Abrahao KP (2018) Synaptic plasticity mechanisms common to learning and alcohol use
867 disorder. Learn Mem 25:425-434.
868 Maienschein V, Marxen M, Volknandt W, Zimmermann H (1999) A plethora of presynaptic proteins
869 associated with ATP-storing organelles in cultured astrocytes. Glia 26:233-244.
870 Minerbi A, Kahana R, Goldfeld L, Kaufman M, Marom S, Ziv NE (2009) Long-term relationships between
871 synaptic tenacity, synaptic remodeling, and network activity. PLoS Biol 7:e1000136.
872 Miyasaka Y, Yamamoto N (2021) Neuronal Activity Patterns Regulate Brain-Derived Neurotrophic Factor
873 Expression in Cortical Cells via Neuronal Circuits. Front Neurosci 15:699583.
874 Nishimune A, Isaac JT, Molnar E, Noel J, Nash SR, Tagaya M, Collingridge GL, Nakanishi S, Henley JM
875 (1998) NSF binding to GluR2 regulates synaptic transmission. Neuron 21:87-97.
876 O'Brien RJ, Kamboj S, Ehlers MD, Rosen KR, Fischbach GD, Huganir RL (1998) Activity-dependent
877 modulation of synaptic AMPA receptor accumulation. Neuron 21:1067-1078.

878 Oh MC, Derkach VA (2005) Dominant role of the GluR2 subunit in regulation of AMPA receptors by
879 CaMKII. Nat Neurosci 8:853-854.
880 Ormel L, Stensrud MJ, Bergersen LH, Gundersen V (2012) VGLUT1 is localized in astrocytic processes in
881 several brain regions. Glia 60:229-238.
882 Osten P, Srivastava S, Inman GJ, Vilim FS, Khatri L, Lee LM, States BA, Einheber S, Milner TA, Hanson PI,
883 Ziff EB (1998) The AMPA receptor GluR2 C terminus can mediate a reversible, ATP-dependent
884 interaction with NSF and alpha- and beta-SNAPs. Neuron 21:99-110.
885 Pastuzyn ED, Shepherd JD (2017) Activity-Dependent Arc Expression and Homeostatic Synaptic Plasticity
886 Are Altered in Neurons from a Mouse Model of Angelman Syndrome. Front Mol Neurosci
887 10:234.
888 Pozo K, Goda Y (2010) Unraveling mechanisms of homeostatic synaptic plasticity. Neuron 66:337-351.
889 Riedel D, Antonin W, Fernandez-Chacon R, Alvarez de Toledo G, Jo T, Geppert M, Valentijn JA, Valentijn
890 K, Jamieson JD, Sudhof TC, Jahn R (2002) Rab3D is not required for exocrine exocytosis but for
891 maintenance of normally sized secretory granules. Mol Cell Biol 22:6487-6497.
892 Rutherford LC, Nelson SB, Turrigiano GG (1998) BDNF has opposite effects on the quantal amplitude of
893 pyramidal neuron and interneuron excitatory synapses. Neuron 21:521-530.
894 Sanderson JL, Scott JD, Dell'Acqua ML (2018) Control of Homeostatic Synaptic Plasticity by AKAP-
895 Anchored Kinase and Phosphatase Regulation of Ca(2+)-Permeable AMPA Receptors. J Neurosci
896 38:2863-2876.
897 Schluter OM, Basu J, Sudhof TC, Rosenmund C (2006) Rab3 superprimes synaptic vesicles for release:
898 implications for short-term synaptic plasticity. J Neurosci 26:1239-1246.
899 Schonn JS, van Weering JR, Mohrmann R, Schluter OM, Sudhof TC, de Wit H, Verhage M, Sorensen JB
900 (2010) Rab3 proteins involved in vesicle biogenesis and priming in embryonic mouse chromaffin
901 cells. Traffic 11:1415-1428.
902 Seeburg DP, Sheng M (2008) Activity-induced Polo-like kinase 2 is required for homeostatic plasticity of
903 hippocampal neurons during epileptiform activity. J Neurosci 28:6583-6591.
904 Shepherd JD, Rumbaugh G, Wu J, Chowdhury S, Plath N, Kuhl D, Huganir RL, Worley PF (2006)
905 Arc/Arg3.1 mediates homeostatic synaptic scaling of AMPA receptors. Neuron 52:475-484.
906 Shinoda Y, Ahmed S, Ramachandran B, Bharat V, Brockelt D, Altas B, Dean C (2014) BDNF enhances
907 spontaneous and activity-dependent neurotransmitter release at excitatory terminals but not at
908 inhibitory terminals in hippocampal neurons. Front Synaptic Neurosci 6:27.
909 Silva MM, Rodrigues B, Fernandes J, Santos SD, Carreto L, Santos MAS, Pinheiro P, Carvalho AL (2019)
910 MicroRNA-186-5p controls GluA2 surface expression and synaptic scaling in hippocampal
911 neurons. Proc Natl Acad Sci U S A 116:5727-5736.
912 Smith-Dijak AI, Nassrallah WB, Zhang LYJ, Geva M, Hayden MR, Raymond LA (2019) Impairment and
913 Restoration of Homeostatic Plasticity in Cultured Cortical Neurons From a Mouse Model of
914 Huntington Disease. Front Cell Neurosci 13:209.
915 Soden ME, Chen L (2010) Fragile X protein FMRP is required for homeostatic plasticity and regulation of
916 synaptic strength by retinoic acid. J Neurosci 30:16910-16921.
917 Song I, Kamboj S, Xia J, Dong H, Liao D, Huganir RL (1998) Interaction of the N-ethylmaleimide-sensitive
918 factor with AMPA receptors. Neuron 21:393-400.
919 Statman A, Kaufman M, Minerbi A, Ziv NE, Brenner N (2014) Synaptic size dynamics as an effectively
920 stochastic process. PLoS Comput Biol 10:e1003846.
921 Stellwagen D, Malenka RC (2006) Synaptic scaling mediated by glial TNF-alpha. Nature 440:1054-1059.
922 Stellwagen D, Beattie EC, Seo JY, Malenka RC (2005) Differential regulation of AMPA receptor and GABA
923 receptor trafficking by tumor necrosis factor-alpha. J Neurosci 25:3219-3228.
924 Suh YH, Terashima A, Petralia RS, Wenthold RJ, Isaac JT, Roche KW, Roche PA (2010) A neuronal role for
925 SNAP-23 in postsynaptic glutamate receptor trafficking. Nat Neurosci 13:338-343.

926 Sutton MA, Ito HT, Cressy P, Kempf C, Woo JC, Schuman EM (2006) Miniature neurotransmission
927 stabilizes synaptic function via tonic suppression of local dendritic protein synthesis. Cell
928 125:785-799.
929 Suzuki K, Kim JW, Nosyreva E, Kavalali ET, Monteggia LM (2021) Convergence of distinct signaling
930 pathways on synaptic scaling to trigger rapid antidepressant action. Cell Rep 37:109918.
931 Takei N, Sasaoka K, Inoue K, Takahashi M, Endo Y, Hatanaka H (1997) Brain-derived neurotrophic factor
932 increases the stimulation-evoked release of glutamate and the levels of exocytosis-associated
933 proteins in cultured cortical neurons from embryonic rats. J Neurochem 68:370-375.
934 Tan HL, Queenan BN, Huganir RL (2015) GRIP1 is required for homeostatic regulation of AMPAR
935 trafficking. Proc Natl Acad Sci U S A 112:10026-10031.
936 Thakker-Varia S, Alder J, Crozier RA, Plummer MR, Black IB (2001) Rab3A is required for brain-derived
937 neurotrophic factor-induced synaptic plasticity: transcriptional analysis at the population and
938 single-cell levels. J Neurosci 21:6782-6790.
939 Thiagarajan TC, Lindskog M, Tsien RW (2005) Adaptation to synaptic inactivity in hippocampal neurons.
940 Neuron 47:725-737.
941 Tian M, Xu CS, Montpetit R, Kramer RH (2012) Rab3A mediates vesicle delivery at photoreceptor ribbon
942 synapses. J Neurosci 32:6931-6936.
943 Tononi G, Cirelli C (2014) Sleep and the price of plasticity: from synaptic and cellular homeostasis to
944 memory consolidation and integration. Neuron 81:12-34.
945 Torrado Pacheco A, Bottorff J, Gao Y, Turrigiano GG (2021) Sleep Promotes Downward Firing Rate
946 Homeostasis. Neuron 109:530-544 e536.
947 Trasande CA, Ramirez JM (2007) Activity deprivation leads to seizures in hippocampal slice cultures: is
948 epilepsy the consequence of homeostatic plasticity? J Clin Neurophysiol 24:154-164.
949 Tsetsenis T, Younts TJ, Chiu CQ, Kaeser PS, Castillo PE, Sudhof TC (2011) Rab3B protein is required for
950 long-term depression of hippocampal inhibitory synapses and for normal reversal learning. Proc
951 Natl Acad Sci U S A 108:14300-14305.
952 Turrigiano GG (1999) Homeostatic plasticity in neuronal networks: the more things change, the more
953 they stay the same. Trends Neurosci 22:221-227.
954 Turrigiano GG, Nelson SB (2004) Homeostatic plasticity in the developing nervous system. Nat Rev
955 Neurosci 5:97-107.
956 Turrigiano GG, Leslie KR, Desai NS, Rutherford LC, Nelson SB (1998) Activity-dependent scaling of
957 quantal amplitude in neocortical neurons. Nature 391:892-896.
958 Wang G, Zhong J, Guttieres D, Man HY (2019) Non-scaling regulation of AMPA receptors in homeostatic
959 synaptic plasticity. Neuropharmacology 158:107700.
960 Wang JKT, Langfelder P, Horvath S, Palazzolo MJ (2017) Exosomes and Homeostatic Synaptic Plasticity
961 Are Linked to Each other and to Huntington's, Parkinson's, and Other Neurodegenerative
962 Diseases by Database-Enabled Analyses of Comprehensively Curated Datasets. Front Neurosci
963 11:149.
964 Wang X, Thiagarajan R, Wang Q, Tewolde T, Rich MM, Engisch KL (2008) Regulation of quantal shape by
965 Rab3A: evidence for a fusion pore-dependent mechanism. J Physiol 586:3949-3962.
966 Wang X, Wang Q, Yang S, Bucan M, Rich MM, Engisch KL (2011) Impaired activity-dependent plasticity of
967 quantal amplitude at the neuromuscular junction of Rab3A deletion and Rab3A earlybird mutant
968 mice. J Neurosci 31:3580-3588.
969 Wang X, Li Y, Engisch KL, Nakanishi ST, Dodson SE, Miller GW, Cope TC, Pinter MJ, Rich MM (2005)
970 Activity-dependent presynaptic regulation of quantal size at the mammalian neuromuscular
971 junction in vivo. J Neurosci 25:343-351.
972 Weisskopf MG, Castillo PE, Zalutsky RA, Nicoll RA (1994) Mediation of hippocampal mossy fiber long-
973 term potentiation by cyclic AMP. Science 265:1878-1882.

974 Wilson NR, Kang J, Hueske EV, Leung T, Varoqui H, Murnick JG, Erickson JD, Liu G (2005) Presynaptic
975 regulation of quantal size by the vesicular glutamate transporter VGLUT1. J Neurosci 25:6221-
976 6234.
977 Wu D, Bacaj T, Morishita W, Goswami D, Arendt KL, Xu W, Chen L, Malenka RC, Sudhof TC (2017)
978 Postsynaptic synaptotagmins mediate AMPA receptor exocytosis during LTP. Nature 544:316-
979 321.
980 Xu X, Pozzo-Miller L (2017) EEA1 restores homeostatic synaptic plasticity in hippocampal neurons from
981 Rett syndrome mice. J Physiol 595:5699-5712.
982 Zhu H, Bhattacharyya B, Lin H, Gomez CM (2013) Skeletal muscle calpain acts through nitric oxide and
983 neural miRNAs to regulate acetylcholine release in motor nerve terminals. J Neurosci 33:7308-
984 7324.

985

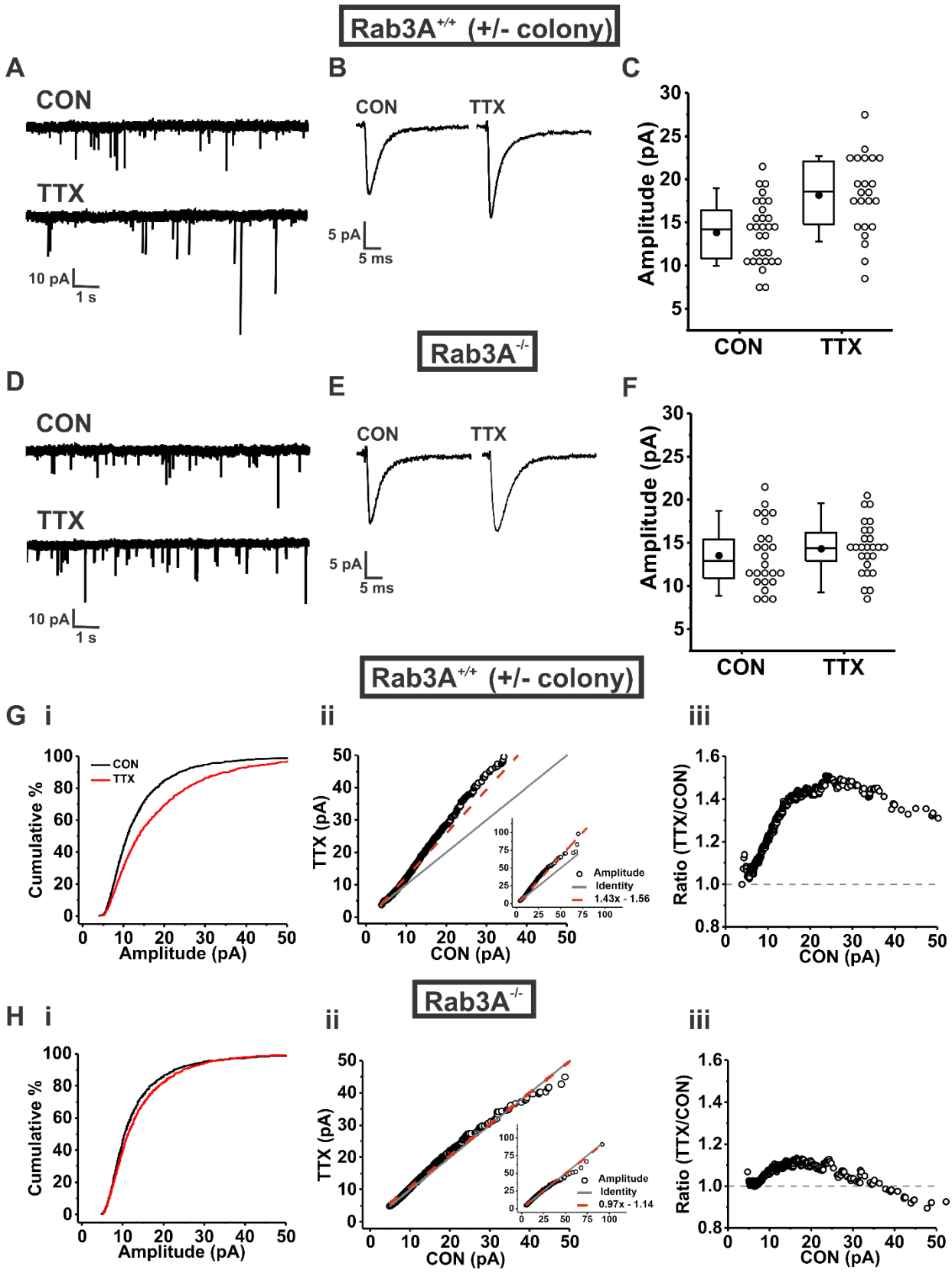
Rab3A+/+ (+/- colony)
A
CON
TTX
10 pA
1 s
B
CON
TTX
5 pA
5 ms
C
Amplitude (pA)
CON
TTX
Rab3A-/-
D
CON
TTX
10 pA
1 s
E
CON
TTX
5 pA
5 ms
F
Amplitude (pA)
CON
TTX
Rab3A+/+ (+/- colony)
G i
Cumulative %
Amplitude (pA)
CON
TTX
ii
TTX (pA)
CON (pA)
Amplitude
Identity
1.43x - 1.56
iii
Ratio (TTX/CON)
CON (pA)
Rab3A-/-
H i
Cumulative %
Amplitude (pA)
ii
TTX (pA)
CON (pA)
Amplitude
Identity
0.97x - 1.14
iii
Ratio (TTX/CON)
CON (pA)

FIGURE 1

988
989
990 Figure 1. Block of activity with 48 hours TTX treatment increased mEPSC amplitudes in cortical
991 cultures from wild type mice but not Rab3A$^{-/-}$ mice. A) 10 second current traces recorded at -60
992 mV in pyramidal cortical neurons from an untreated ("CON") and TTX-treated ("TTX") neuron in
993 cultures prepared from Rab3A$^{+/+}$ mice from the Rab3A$^{+/-}$ colony. B) Average traces for the
994 recordings shown in (A). C) Box and whisker plots for average mEPSC amplitudes from 30 CON
995 and 23 TTX cells (Rab3A$^{+/+}$, Rab3A$^{+/-}$ colony; mean mEPSC amplitudes, CON, 13.9 ± 0.7 pA; TTX,
996 18.2 ± 0.9 pA, $p = 4.58 * 10^{-4}$, Kruskal-Wallis test). D) Current traces recorded in pyramidal
997 cortical neurons from a CON and TTX-treated neuron in cultures prepared from Rab3A$^{-/-}$ mice.
998 E) Average traces for the recordings shown in (D). F) Box and whisker plots for average mEPSC
999 amplitudes from 25 CON and 26 TTX cells, Rab3A$^{-/-}$ data (Rab3A$^{-/-}$, mean mEPSC amplitudes,
1000 CON, 13.6 ± 0.1; TTX, 14.3 ± 0.6, p = 0.318, Kruskal-Wallis test). G) Analysis of pooled mEPSC
1001 amplitudes for cultures from Rab3A$^{+/+}$ mice of the Rab3A$^{+/-}$ colony (i) Cumulative distribution
1002 functions (CDFs) of quantiles of mEPSC amplitudes pooled from CON (black curve) and TTX-
1003 treated cultures (red curve) (Kolmogorov Smirnov (KS) test, test statistic (D) = 0.149, $p = 8.53 *$
1004 10^{-13}. (ii) Quantiles pooled from CON and TTX-treated cells were ranked from smallest to
1005 largest, plotted against each other, and fit with linear regression functions. Gray line, identity;
1006 red dashed line, linear regression fit. Inset, full range of the data. (iii) The same ranked mEPSC
1007 quantiles were paired and the ratio of CON/TTX computed for each pair, then plotted as a
1008 function of the CON mEPSC for the pair. Dashed line at ratio = 1.0 (no plasticity). H) Analysis of
1009 pooled mEPSCs amplitudes for cultures from Rab3A$^{-/-}$ mice. (i) CDFs of quantiles pooled from
1010 CON (black curve) and TTX-treated cultures (red curve) (KS test, D = 0.070, p = 0.042). (ii)
1011 Quantiles pooled from CON and TTX-treated cells were ranked from smallest to largest, plotted
1012 against each other, and fit with a linear regression function. Gray lines, identity; red dashed
1013 lines, linear regression fits. Inset: full range of the data. (iii) The same ranked mEPSC quantiles
1014 were paired and the ratio of CON/TTX computed for each pair, then plotted as a function of the
1015 CON mEPSC for the pair. Dashed line at ratio = 1 (no plasticity).
1016

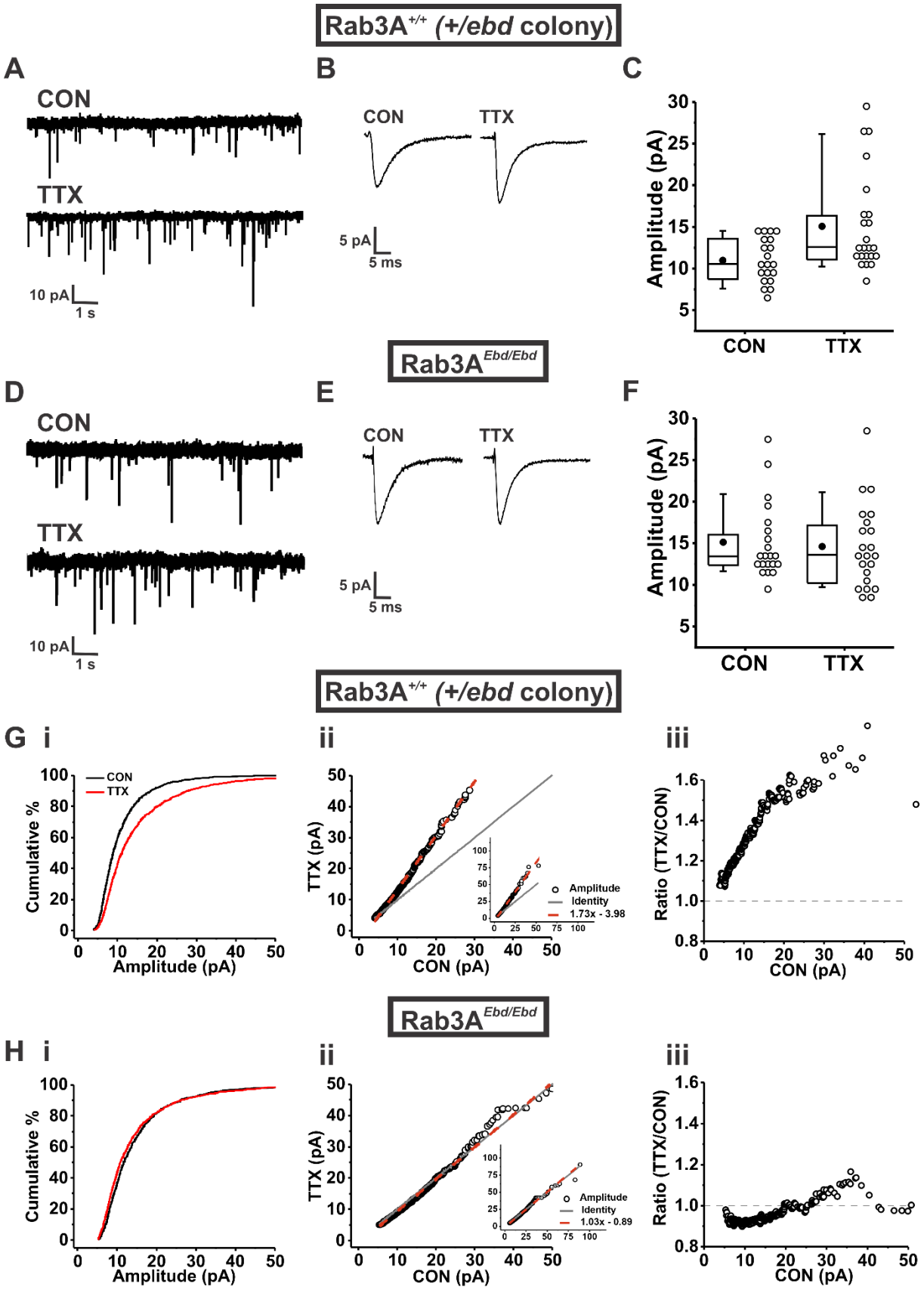
Rab3A+/+ (+/ebd colony)
A
CON
TTX
10 pA
1 s
B
CON
TTX
5 pA
5 ms
C
Amplitude (pA)
CON
TTX
Rab3A Ebd/Ebd
D
CON
TTX
10 pA
1 s
E
CON
TTX
5 pA
5 ms
F
Amplitude (pA)
CON
TTX
Rab3A+/+ (+/ebd colony)
G i
CON
TTX
Cumulative %
Amplitude (pA)
ii
TTX (pA)
CON (pA)
Amplitude
Identity
1.73x - 3.98
iii
Ratio (TTX/CON)
CON (pA)
Rab3A Ebd/Ebd
H i
Cumulative %
Amplitude (pA)
ii
TTX (pA)
CON (pA)
Amplitude
Identity
1.03x - 0.89
iii
Ratio (TTX/CON)
CON (pA)

FIGURE 2

1018

1019 Figure 2. Block of activity with 48 hours TTX treatment increased mEPSC amplitudes in cortical
1020 cultures from wild type mice but not Rab3A$^{Ebd/Ebd}$ mice, which had an increased mEPSC
1021 amplitude at baseline. A) 10 second current traces recorded at -60 mV in pyramidal cortical
1022 neurons from an untreated ("CON") and TTX-treated ("TTX") neuron in cultures prepared from
1023 Rab3A$^{+/+}$ mice from the Rab3A$^{+/Ebd}$ colony. B) Average traces for the recordings shown in (A). C)
1024 Box and whisker plots for average mEPSC amplitudes from 20 CON and 23 TTX cells (Rab3A$^{+/+}$,
1025 Rab3A$^{+/Ebd}$ colony, mean mEPSCs amplitudes, CON, 11.0 ± 0.6 pA; TTX, 15.0 ± 1.3 pA, p = 0.02,
1026 Kruskal-Wallis test). D) Current traces recorded in pyramidal-shaped cortical neurons from a
1027 CON and TTX-treated neuron in cultures prepared from Rab3A$^{Ebd/Ebd}$ mice. E) Average traces for
1028 the recordings shown in (D). F) Box and whisker plots of average mEPSC amplitudes from 21
1029 CON and 22 TTX cells (Rab3A$^{Ebd/Ebd}$, mean mEPSC amplitudes, CON, 15.1 ± 1.0 pA; TTX, 14.6 ±
1030 1.1 pA, p = 0.81, Kruskal-Wallis test). G) Analysis of pooled mEPSC amplitudes for cultures from
1031 Rab3A$^{+/+}$ mice of the Rab3A$^{+/Ebd}$ colony. (i) CDFs of quantiles pooled from CON (black curve) and
1032 TTX-treated cultures (red curve) (KS test, D = 0.177, p value = 2.88 * 10^{-9}). (ii) Quantiles pooled
1033 from CON and TTX-treated cells were ranked from smallest to largest, plotted against each
1034 other, and fit with linear regression function. Gray line, identity; red dashed line, linear
1035 regression fit. Inset: full range of the data. (iii) The same ranked mEPSC quantiles were paired
1036 and the ratio of CON/TTX computed for each pair, then plotted as a function of the CON mEPSC
1037 for the pair. Dashed line at ratio = 1 (no plasticity). H) Analysis of pooled mEPSC amplitudes for
1038 cultures from Rab3A$^{Ebd/Ebd}$ mice. (i) CDFs of quantiles pooled from CON (black curve) and TTX-
1039 treated cultures (red curve). (KS test, D = 0.067, p value = 0.097 (TTX mEPSCs were slightly
1040 *reduced*)). (ii) Quantiles pooled from CON and TTX-treated cells were ranked from smallest to
1041 largest, plotted against each other, and fit with a linear regression function. Gray line, identity;
1042 red dashed line, linear regression fit. Inset: full range of the data. (iii) The same ranked mEPSC
1043 quantiles were paired and the ratio of CON/TTX computed for each pair, then plotted as a
1044 function of the CON mEPSC for the pair. Dashed line at ratio = 1 (no plasticity).

1045

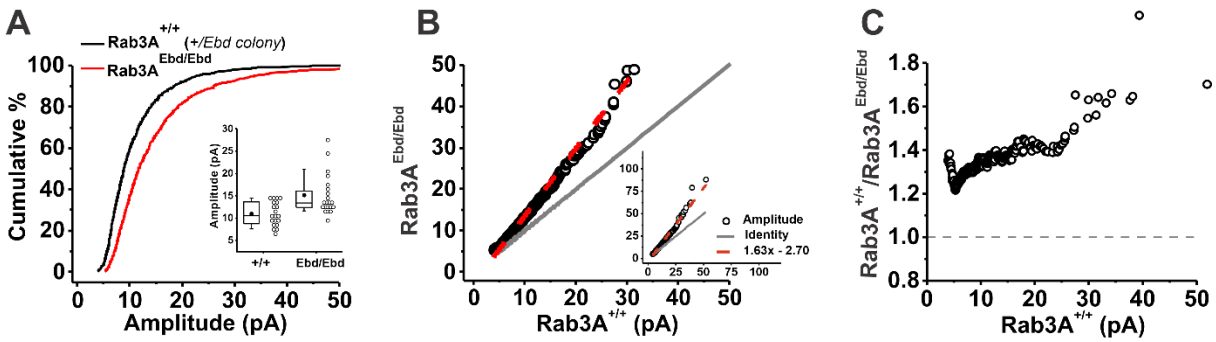

FIGURE 3

Figure 3. The increase in mEPSC amplitudes in neurons from cultures prepared from Rab3A$^{Ebd/Ebd}$ mice, relative to those from Rab3A$^{+/+}$ mice in the same strain, showed less divergent scaling than that of the activity-block induced increase in mEPSC amplitudes typically observed in cultures from Rab3A$^{+/+}$ mice. A) Cumulative distribution function of quantiles pooled from Rab3A$^{+/+}$ (black curve) and Rab3A$^{Ebd/Ebd}$ cultures (red curve), D = 0.245; p = 1.52 * 10^{-16}, KS test. *Inset*: box and whisker plot of average mEPSC amplitudes from 20 Rab3A$^{+/+}$ and 21 Rab3A$^{Ebd/Ebd}$ cells, mean mEPSC amplitudes, Rab3A$^{+/+}$, 11.0 ± 0.7 pA; Rab3A$^{Ebd/Ebd}$, 15.1 ± 1.0 pA, p = 0.0027, Kruskal-Wallis test. B) Quantiles pooled from Rab3A$^{+/+}$ and Rab3A$^{Ebd/Ebd}$ cells were ranked from smallest to largest, plotted against each other, and fit with linear regression functions. Gray line, identity; red dashed line, linear regression fit. C) The same ranked mEPSC quantiles were paired and the ratio of Rab3A$^{+/+}$/Rab3A$^{Ebd/Ebd}$ computed for each pair, then plotted as a function of the Rab3A$^{+/+}$ mEPSC for the pair. Dashed line at ratio = 1.0 (no difference).

1064

1065

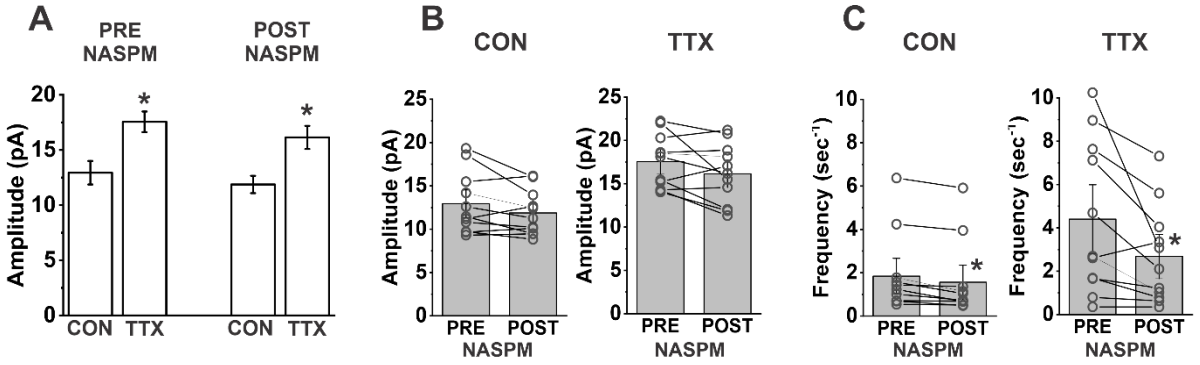

1066

1067 FIGURE 4

1068

1069 Figure 4. Ca^{2+}-permeable, NASPM-sensitive glutamate receptors did not mediate the TTX-
1070 induced increase in mEPSC amplitude in cultures of dissociated mouse cortical neurons. A)
1071 mEPSC amplitudes for 11 mouse cortical neurons from untreated cultures ("CON") and 11
1072 neurons from TTX treated cultures ("TTX") were recorded before and after application of 20 μM
1073 NASPM. mEPSC amplitudes were still significantly larger in TTX-treated cultures compared to
1074 untreated control cultures after NASPM treatment (TTX effect pre-NASPM, p = 0.009; TTX effect
1075 post-NASPM, p = 0.006, Kruskal-Wallis non-parametric test). B) Acute application of NASPM had
1076 a modest effect on mEPSC amplitude in cells from CON or TTX cultures that did not reach
1077 statistical significance (CON, pre-NASPM, 12.9 ± 1.1 pA, post-NASPM, 11.9 ± 0.8 pA, p = 0.08;
1078 TTX, pre-NASPM, 17.5 ± 0.9 pA, post-NASPM, 16.1 ± 1.0 pA, p = 0.08; student's paired t-test). C)
1079 Acute application of NASPM consistently reduced mEPSC frequency in cells from untreated and
1080 cells from TTX-treated cultures (CON, pre-NASPM, 1.84 ± 1.82 mEPSCs sec^{-1}, post-NASPM, 1.56
1081 ± 1.74 mEPSCs sec^{-1}; p = 0.003; TTX, pre-NASPM, 4.40 ± 3.51 mEPSCs sec^{-1}, post-NASPM, 2.68 ±
1082 2.25 mEPSCs sec^{-1}, p = 0.02; student's paired t-test).

1083

1084

1085

1086

1087

1088

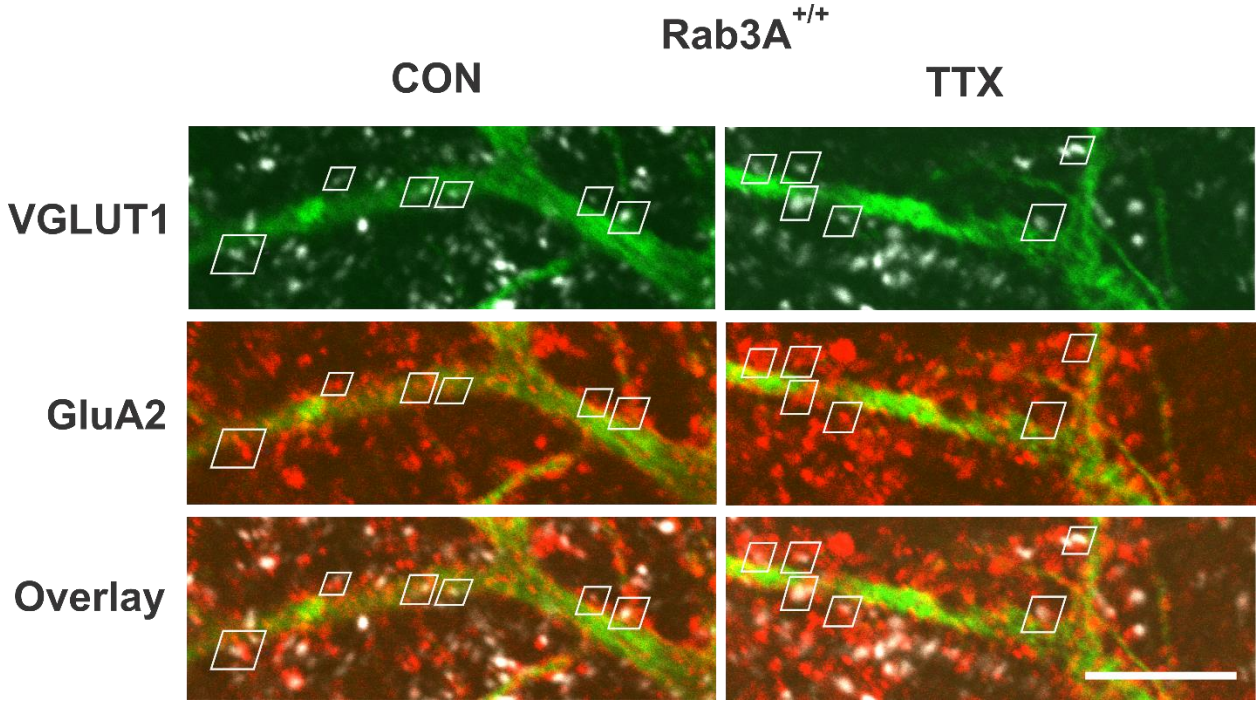

1089

1090 FIGURE 5

1091

1092 Figure 5. Confocal images of GluA2 and VGLUT1 immunofluorescence on MAP2-positive
1093 primary dendrites of pyramidal-shaped neurons in high density dissociated cortical cultures
1094 prepared from Rab3A$^{+/+}$ mice. Shown are 5X confocal sections of two primary dendrites, one
1095 from an untreated culture (CON) and the other from a culture treated with TTX (TTX).
1096 Postsynaptic GluA2-positive receptor clusters were identified by their proximity to VGLUT1
1097 immunoreactive presynaptic terminals within the same confocal section. GluA2-VGLUT1
1098 synaptic pairs, which were of maximal brightness in these confocal slices, are indicated by white
1099 trapezoids. It can be seen that substantial numbers of GluA2-positive clusters located on the
1100 dendrites are unopposed by VGLUT1-positive terminals, and that some GluA2-positive and
1101 VGLUT1-positive clusters are found away from any MAP2 positivity, suggesting localization to
1102 axons or astrocytes. Scale bar = 10 μm.

1103

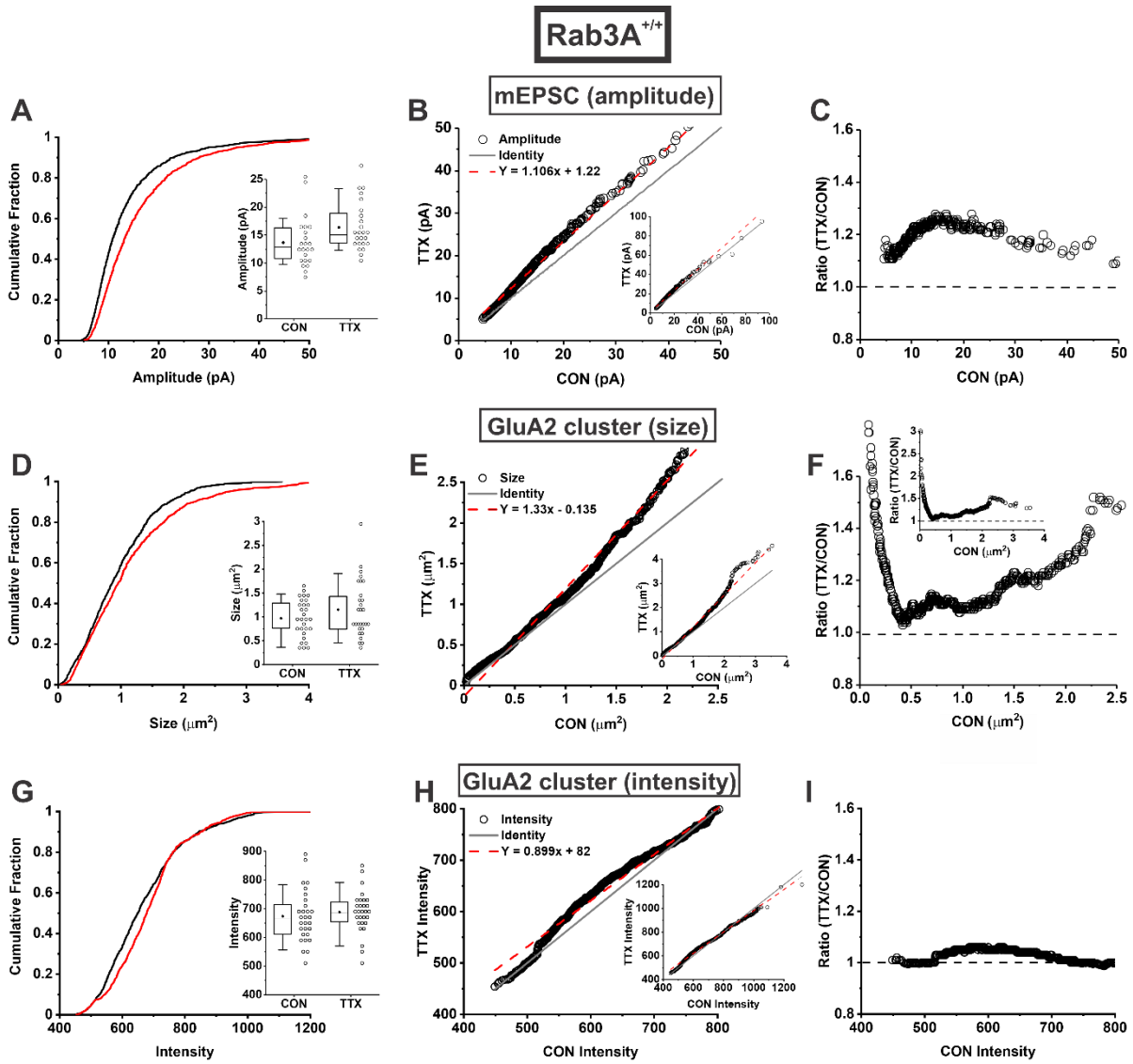
Rab3A+/+
mEPSC (amplitude)
A
B
C
Cumulative Fraction
Amplitude (pA)
CON
TTX
Amplitude
Identity
Y = 1.106x + 1.22
TTX (pA)
CON (pA)
Ratio (TTX/CON)
GluA2 cluster (size)
D
E
F
Size (μm²)
Size
Y = 1.33x - 0.135
TTX (μm²)
CON (μm²)
GluA2 cluster (intensity)
G
H
I
Intensity
Y = 0.899x + 82
TTX Intensity
CON Intensity

FIGURE 6

1106 Figure 6. GluA2 receptor cluster size and average intensity increased following activity blockade
1107 in parallel with mEPSC amplitudes recorded in the same cortical cultures prepared from
1108 Rab3A$^{+/+}$ mice, but the effects on receptor levels were less robust and differed from mEPSC
1109 amplitudes in characteristics of scaling. A) Cumulative distribution functions (CDFs) of mEPSC
1110 amplitudes recorded from untreated ("CON") and TTX-treated cells ("TTX") pooled from 3
1111 cultures were significantly different (KS test, D = 0.162, p = 1.42 * 10^{-8}, CON, n = 690, TTX, n =
1112 720). *Inset*, mean mEPSC amplitudes for 23 CON cells and 24 TTX cells were significantly
1113 different (CON, 13.7 ± 4.5 pA; TTX, 16.4 ± 4.3 pA, p = 0.016, Kruskal-Wallis test). B) 24 mEPSC
1114 amplitude quantiles from each of 23 untreated cells were sorted from smallest to largest and
1115 plotted vs. 23 mEPSC amplitude quantiles from each of 24 TTX-treated cells, and the resulting
1116 relationship fit with a linear regression equation, Y = 1.106x + 1.22 (R^2 = 0.984). *Inset*, full range
1117 of data used for fit. C) Sorted data from (B) were used to calculate the ratio of TTX mEPSC
1118 amplitude/CON mEPSC amplitude and the ratios plotted vs. CON mEPSC amplitude. D) CDFs of
1119 size of GluA2 receptor clusters imaged from primary dendrites in the same untreated cultures
1120 and TTX-treated cultures as in (A) – (C) were significantly different (KS test, D = 0.089, p = 0.002,
1121 CON, n = 870, TTX, n = 870). *Inset*, mean GluA2 cluster size for 29 CON dendrites and 29 TTX
1122 dendrites were not significantly different (CON, 0.97 ± 0.38 μm^2; TTX, 1.15 ± 0.59 μm^2, p = 0.44,
1123 Kruskal-Wallis test). E) 29 GluA2 cluster size quantiles from each of 29 untreated dendrites
1124 were sorted from smallest to largest and plotted vs. 29 cluster size quantiles from each of 29
1125 TTX-treated dendrites, and the resulting relationship fit with a linear regression equation, Y =
1126 1.328x -0.136 (R^2 = 0.98). *Inset*, full range of data used for fit. F) Sorted data from (E) were used
1127 to calculate the ratio of TTX GluA2 cluster size/CON GluA2 cluster size and the ratios plotted vs.
1128 CON GluA2 cluster size. G) CDFs of intensity of GluA2 receptor clusters imaged from primary
1129 dendrites in untreated cultures and TTX-treated cultures were significantly different (KS test, D
1130 = 0.120, p = 6.73 * 10^{-6}, CON, n = 870, TTX, n = 870). *Inset*, mean GluA2 cluster intensity for 29
1131 CON dendrites and 29 TTX dendrites were not significantly different (CON, 673 ± 90 a.u.; TTX,
1132 687 ± 72 a.u., p = 0.25, Kruskal-Wallis test). H) 29 GluA2 cluster intensity quantiles from 29
1133 untreated dendrites were sorted from smallest to largest and plotted vs. 29 cluster intensity
1134 quantiles from 29 TTX-treated dendrites, and the resulting relationship fit with a linear
1135 regression equation, Y = 0.899x + 82 (R^2 = 0.987). *Inset*, full range of data used for fit. I) Sorted
1136 data from (H) were used to calculate the ratio of TTX cluster intensity/CON cluster intensity and
1137 plotted vs. CON cluster intensity.

1138

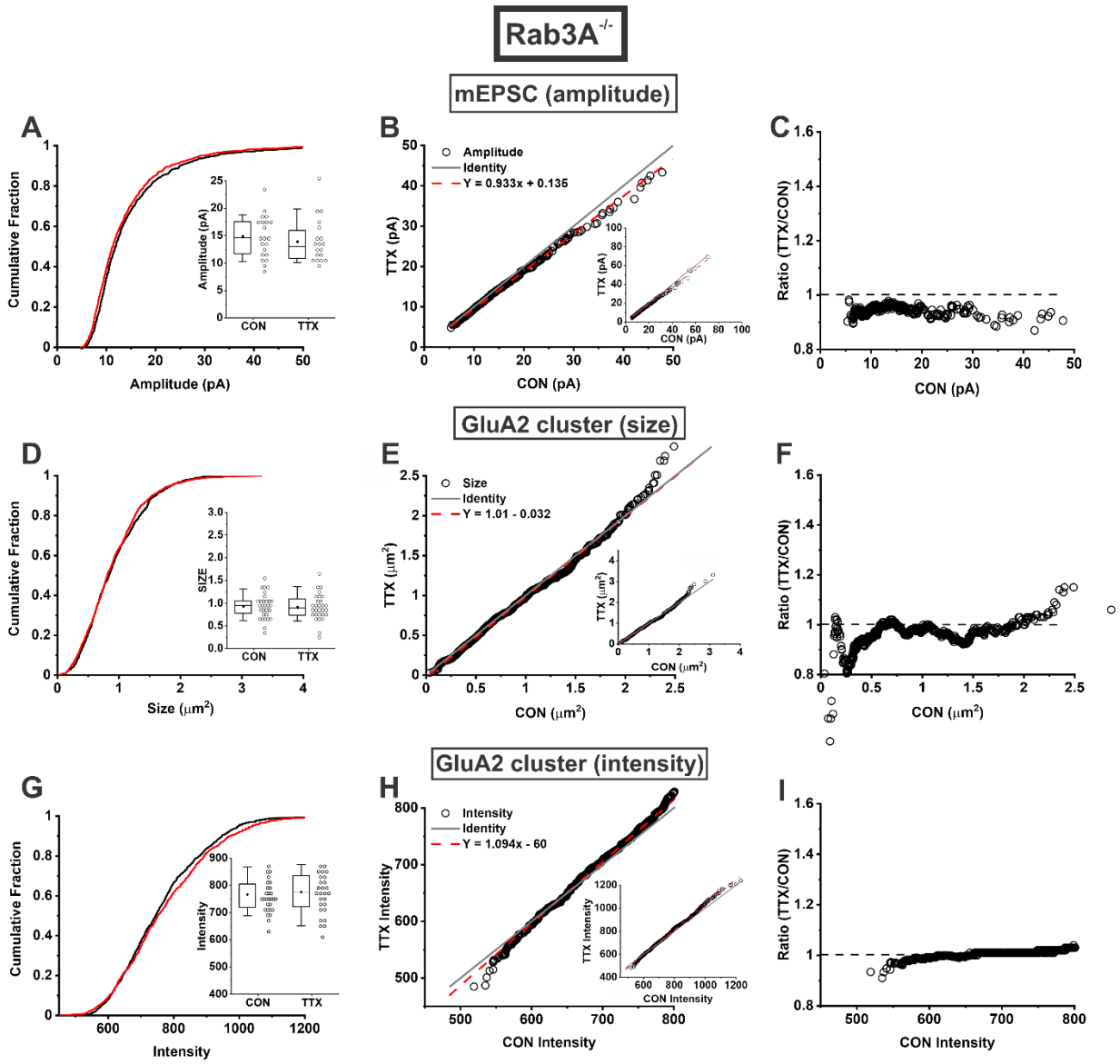
Rab3A-/-
mEPSC (amplitude)
A
Cumulative Fraction
Amplitude (pA)
CON
TTX
B
Amplitude
Identity
Y = 0.933x + 0.135
TTX (pA)
CON (pA)
C
Ratio (TTX/CON)
CON (pA)
GluA2 cluster (size)
D
Cumulative Fraction
SIZE
Size (μm²)
E
Size
Identity
Y = 1.01 - 0.032
TTX (μm²)
CON (μm²)
F
Ratio (TTX/CON)
CON (μm²)
GluA2 cluster (intensity)
G
Cumulative Fraction
Intensity
H
Intensity
Identity
Y = 1.094x - 60
TTX Intensity
CON Intensity
I
Ratio (TTX/CON)
CON Intensity

FIGURE 7

1141 Figure 7. GluA2 receptor cluster size, average intensity, and mEPSC amplitudes recorded in the
1142 same cortical cultures prepared from Rab3A$^{-/-}$ mice were not increased following activity
1143 blockade. A) Cumulative distribution functions (CDFs) of mEPSC amplitudes recorded from
1144 untreated ("CON") and TTX-treated cells ("TTX") pooled from 3 Rab3A$^{-/-}$ cultures were not
1145 significantly different (KS test, D = 0.072, p = 0.085, CON, n = 630, TTX, n = 570). *Inset*, mean
1146 mEPSC amplitudes for 21 CON cells and 19 TTX cells were not significantly different (CON, 14.9
1147 ± 3.8 pA; TTX, 14.0 ± 4.0 pA, p = 0.34, Kruskal-Wallis test). B) 19 mEPSC quantiles from each of
1148 21 untreated cells were sorted from smallest to largest and plotted vs. 21 mEPSC quantiles
1149 from each of 19 TTX-treated cells, and the resulting relationship fit with a linear regression
1150 equation, Y = 0.93x + 0.13 (R^2 = 0.997). *Inset*, full range of data used for fit. C) Sorted data from
1151 (B) were used to calculate the ratio of TTX mEPSC amplitude/CON mEPSC amplitude and
1152 plotted vs. CON mEPSC amplitude. D) CDFs of GluA2 receptor cluster size imaged from primary
1153 dendrites in the same untreated cultures and TTX-treated cultures as in (A) – (C) were not
1154 significantly different (KS test, D = 0.045, p = 0.31, CON, n = 900, TTX, n = 870). *Inset*, mean
1155 GluA2 cluster size for 30 CON dendrites and 29 TTX dendrites were not significantly different
1156 (CON, 0.93 ± 0.27 μm^2; TTX, 0.91 ± 0.28 μm^2, p = 0.74, Kruskal-Wallis test). E) 29 GluA2 cluster
1157 size quantiles from each of 30 untreated dendrites were sorted from smallest to largest and
1158 plotted vs. 30 cluster size quantiles from each of 29 TTX-treated dendrites, and the resulting
1159 relationship fit with a linear regression equation, Y = 1.01x -0.03 (R^2 = 0.993). *Inset*, full range of
1160 data used for fit. F) Sorted data from (E) were used to calculate the ratio of TTX GluA2 cluster
1161 size/CON GluA2 cluster size and the ratios plotted vs. CON GluA2 cluster size. G) CDFs of GluA2
1162 receptor cluster average intensity imaged from primary dendrites in untreated cultures and
1163 TTX-treated cultures were not significantly different (KS test, D = 0.0.060, p = 0.08, CON, n =
1164 900, TTX, n = 870). *Inset*, mean GluA2 cluster intensity for 30 CON dendrites and 29 TTX
1165 dendrites were not significantly different (CON, 766 ± 68 a.u.; TTX, 776 ± 79 a.u., p = 0.47,
1166 Kruskal-Wallis test). H) 29 GluA2 cluster intensity quantiles from 30 untreated dendrites were
1167 sorted from smallest to largest and plotted vs. 30 cluster intensity quantiles from 29 TTX-
1168 treated dendrites, and the resulting relationship fit with a linear regression equation, Y = 1.09x -
1169 60 (R^2 = 0.993). *Inset*, full range of data used for fit. I) Sorted data from (H) were used to
1170 calculate the ratio of TTX cluster intensity/CON cluster intensity and the ratios plotted vs. CON
1171 cluster intensity.

1172

1173

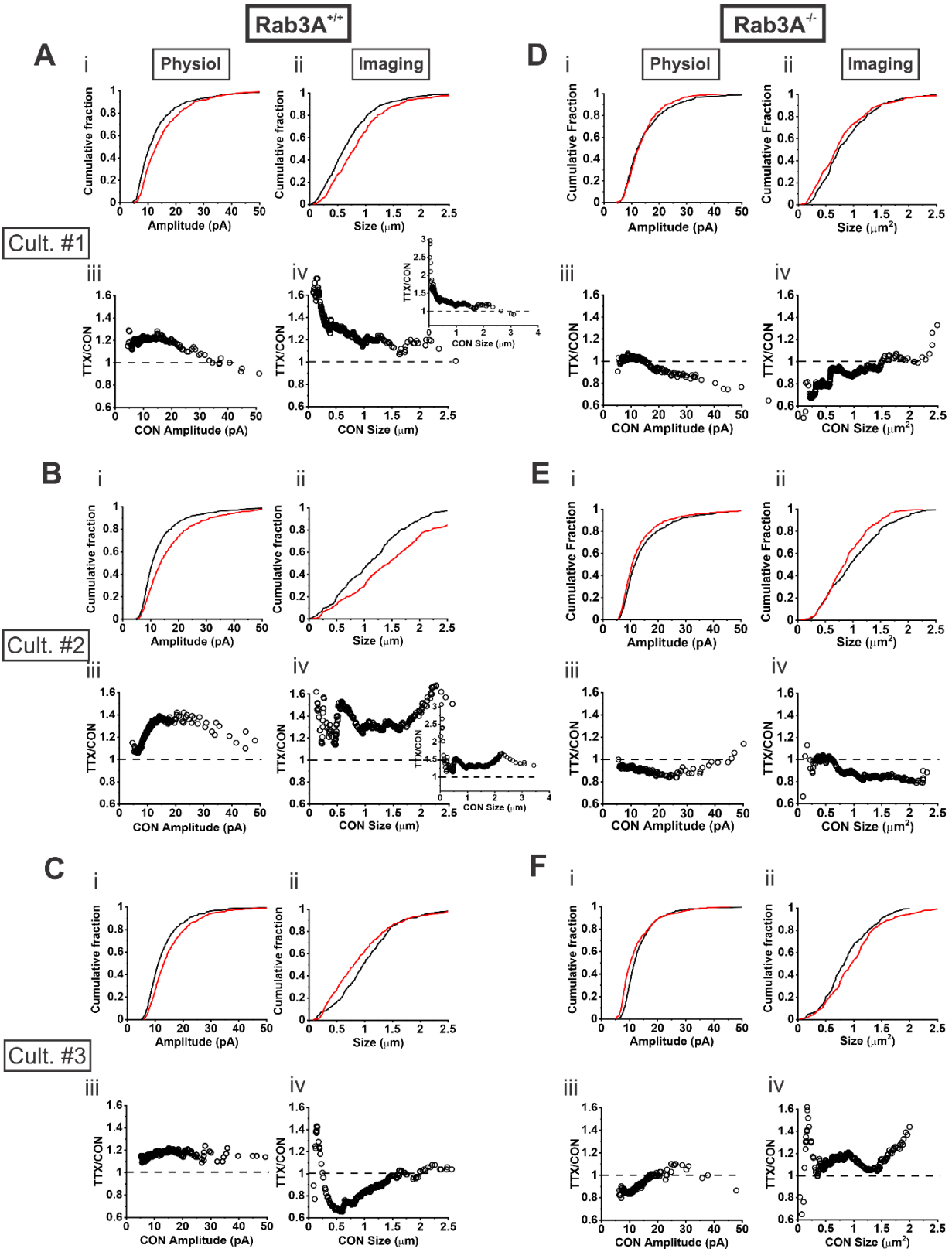

1174 FIGURE 8

Figure 8. mEPSC amplitudes and GluA2 receptor cluster sizes did not always change in parallel after treatment with TTX in cultures from Rab3A$^{+/+}$ and Rab3A$^{-/-}$ mice. A) **Rab3A$^{+/+}$ Culture #1**: mEPSC amplitudes and GluA2 receptor cluster sizes increased in parallel after treatment in TTX. i) CDFs of mEPSC amplitudes of cells from untreated and TTX treated dishes were significantly different (KS test, D = 0.16, p = 0.010; CON, n = 180, TTX, n = 210). ii) CDFs of GluA2 receptor cluster sizes of dendrites from untreated and TTX treated dishes were significantly different (KS test, D = 0.17, p = 3.79 * 10^{-4}; CON, n = 300, TTX, n = 300). iii) 35 mEPSC amplitude quantiles from each of 6 untreated cells and 30 quantiles from each of 7 TTX-treated cells were sorted from smallest to largest and used to calculate the ratio of TTX mEPSC amplitude/CON mEPSC amplitude, which was plotted vs. CON mEPSC amplitude. iv) 30 GluA2 receptor cluster size quantiles from each of 10 untreated dendrites and 30 GluA2 receptor cluster size quantiles from each of 10 TTX-treated dendrites were used to calculate the ratio of TTX GluA2 cluster size/CON GluA2 cluster size, and plotted vs. CON GluA2 cluster size. *Inset*, full range of data. B) **Rab3A$^{+/+}$ Culture #2:** mEPSC amplitudes and GluA2 receptor cluster sizes increased in parallel after treatment in TTX. i) CDFs of mEPSC amplitudes of cells from untreated and TTX treated dishes were significantly different (KS test, D = 0.21, p = 1.06 * 10^{-4}; CON, n = 210, TTX, n = 240). ii) CDFs of GluA2 receptor cluster sizes of dendrites from untreated and TTX treated dishes were significantly different (KS test, D = 0.21, p = 5.39 * 10^{-6}; CON, n = 270, TTX, n = 300). iii) 32 mEPSC amplitude quantiles from each of 7 untreated cells, and 28 mEPSC amplitude quantiles from each of 8 TTX treated cells were sorted from smallest to largest and were used to calculate the ratio of TTX mEPSC amplitude/CON mEPSC amplitude, and plotted vs. CON mEPSC amplitude. iv) 30 GluA2 receptor cluster size quantiles from each of 9 untreated dendrites and 27 GluA2 receptor cluster size quantiles from each of 10 TTX-treated dendrites were sorted from smallest to largest and used to calculate the ratio of TTX GluA2 cluster/CON GluA2 cluster size, and plotted vs. CON GluA2 cluster size. *Inset*, full range of data. C) **Rab3A$^{+/+}$ Culture #3**: mEPSC amplitudes increased, but GluA2 receptor cluster sizes decreased, after treatment in TTX. i) CDFs of mEPSC amplitudes of cells from untreated and TTX treated dishes were significantly different (KS test, D = 0.15, p = 0.002; CON, n = 300, TTX, n = 270). ii) CDFs of GluA2 receptor cluster sizes of dendrites from untreated and TTX treated dishes were significantly different, but the TTX CDF is shifted to the *left* (KS test, D = 0.16, p = 0.001; CON, n = 300, TTX, n = 270) iii) 27 mEPSC amplitude quantiles from each of 10 untreated cells, and 30 mEPSC amplitude quantiles from each of 9 TTX-treated cells, were sorted from smallest to largest, used to calculate the ratio of TTX mEPSC amplitude/ CON mEPSC amplitude, and plotted vs. CON mEPSC amplitude. **iv)** 27 GluA2 receptor cluster size quantiles from each of 10 untreated dendrites and 30 GluA2 receptor cluster sizes from each of 9 TTX-treated dendrites were sorted from smallest to largest, used to calculate the ratio of TTX GluA2 receptor cluster size/CON GluA2 receptor cluster size, and plotted vs. CON GluA2 receptor cluster size. D) **Rab3A$^{-/-}$ Culture #1** (note, this culture is distinct from that of Rab3A$^{+/+}$ Culture #1). Neither mEPSC amplitudes, nor GluA2 receptor cluster size, increased following TTX treatment. i) CDFs of mEPSC amplitudes of cells from untreated and TTX-treated cultures were not significantly different (KS test, D = 0.05, p = 0.90; CON, n = 210, TTX, n = 180). ii) CDFs of GluA2 receptor cluster sizes of dendrites from untreated and TTX (Figure 8 continued) treated dishes were not significantly different, although the TTX CDF is shifted slightly to the *left* (KS test, D = 0.10, p = 0.08; CON, n = 300, TTX, n = 300). iii) 30 mEPSC amplitude quantiles from each of 7 untreated cells and 35

mEPSC quantiles from each of 6 TTX-treated cells were sorted from smallest to largest, used to calculate the ratio TTX mEPSC amplitude/CON mEPSC amplitude, and plotted vs. CON mEPSC amplitude. iv) 30 GluA2 receptor cluster size quantiles from each of 10 untreated dendrites and 10 TTX-treated dendrites were sorted from smallest to largest, used to calculate the ratio TTX cluster size/CON cluster size, and plotted vs. CON cluster size. E) **Rab3A$^{-/-}$ Culture #2** (distinct from Rab3A$^{+/+}$ Culture #2) mEPSC amplitudes and GluA2 receptor cluster sizes decreased after TTX treatment. i) TTX mEPSC amplitudes CDF is shifted slightly to the *left* compared to the CON mEPSC amplitudes CDF but the difference is not significant (KS test, D = 0.08, p = 0.28, CON, n = 240, TTX, n = 240). ii) TTX GluA2 receptor cluster sizes CDF is significantly shifted to the *left* compared to CON GluA2 receptor cluster sizes CDF (KS test, D = 0.13, p = 0.01; CON, n = 300, TTX, n = 300). iii) 24 mEPSC amplitude quantiles from each of 8 untreated cells and 8 TTX-treated cells were sorted from smallest to largest, used to calculate the ratio TTX mEPSC amplitude/CON mEPSC amplitude, and plotted vs. CON mEPSC amplitude. iv) 27 GluA2 receptor cluster size quantiles from each of 10 untreated dendrites, and 30 GluA2 receptor cluster size quantiles from each of 9 TTX treated dendrites, were sorted from smallest to largest, used to calculate the ratio TTX GluA2 cluster size/CON cluster size, and plotted vs. CON cluster size. Both mEPSC amplitude and GluA2 receptor cluster size ratios were below 1 across the majority of data. F) **Rab3A$^{-/-}$ Culture #3** (distinct from Rab3A$^{+/+}$ Culture #3). mEPSC amplitudes were decreased following TTX treatment, but GluA2 receptor cluster sizes were increased. i) TTX CDF of mEPSC amplitudes was significantly shifted to the left of CON CDF (KS test, D = 0.21, p = 4.85 * 10^{-4}, CON, n = 180, TTX, n = 180). ii) TTX CDF of GluA2 receptor cluster sizes was significantly shifted to the right of CON CDF (KS test, D = 0.15, p = 0.003, CON, n = 300, TTX, n = 300). iii) 30 mEPSC amplitude quantiles from each of 6 untreated and 6 TTX-treated cells were sorted from smallest to largest, used to calculate the ratio TTX mEPSC amplitude/CON mEPSC amplitude, and plotted vs. CON mEPSC amplitude. iv) 30 GluA2 receptor cluster size quantiles from each of 10 untreated dendrites and 10 TTX-treated dendrites were sorted from smallest to largest, used to calculate the ratio TTX GluA2 cluster size/CON GluA2 cluster size, and plotted vs. CON CluA2 cluster size.

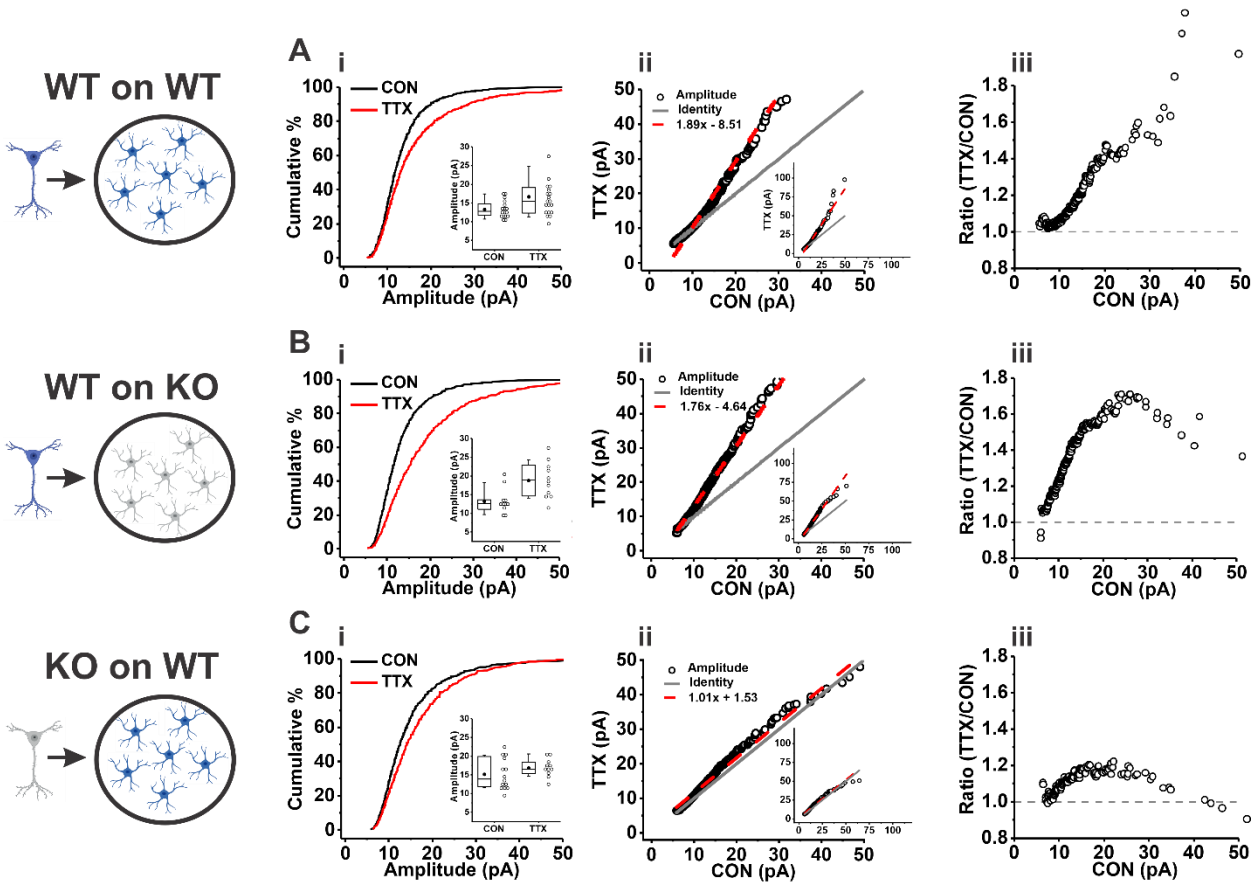

FIGURE 9

Figure 9. Rab3A in neurons, not astrocytes, was required for full homeostatic plasticity after activity blockade. A-C, Data from dissociated cortical neurons plated on an astrocyte feeder layer, each prepared separately from the type of mice depicted in the schema at left: A) Neurons from Rab3A$^{+/+}$ mice plated on astrocytes from Rab3A$^{+/+}$ mice; i) CDFs for mEPSC amplitudes from untreated (CON, black curve) and TTX-treated (TTX, red curve) cultures (KS test, test statistic, D = 0.141, p = 2.74 * 10^{-5}, n = 510 CON, 600 TTX samples; *inset*, means, CON, 13.3 ± 0.5 pA, n = 17 cells, TTX, 16.7 ± 1.2 pA, n = 20 cells, p = 0.03, Kruskal Wallis test; ii) rank order plot and linear regression fit, slope = 1.89, intercept = -8.51, R^2 = 0.97; iii) ratio plot of TTX mEPSC amplitude/CON amplitude vs. CON amplitude; B) Neurons from Rab3A$^{+/+}$ mice plated on astrocytes from Rab3A$^{-/-}$ mice; i) CDFs of mEPSC amplitudes, CON, black curve; TTX, red curve (KS test, test statistic 0.273, p = 2.98 * 10^{-11}), n = 330 CON, 330 TTX samples; *inset*, means, CON, 13.3 ± 1.0 pA, n = 11 cells, TTX, 18.8 ± 1.4 pA, n = 11 cells, p = 0.005, Kruskal-Wallis test; ii) rank order plot and linear regression fit, slope = 1.76, intercept = -4.64, R^2 = 0.98; iii) ratio plot of TTX mEPSC amplitude/TTX mEPSC amplitude vs. CON mEPSC amplitude; C) Neurons from Rab3A$^{-/-}$ neurons plated on astrocytes from Rab3A$^{+/+}$ mice; i) CDFs of mEPSC amplitudes, CON, black curve, TTX, red curve (KS test, test statistic 0.126, p = 0.005), n = 420 CON, 330 TTX samples; *inset*, means, CON, 15.2 ± 1.1 pA, n = 14 cells, TTX, 16.9 ± 0.7 pA, n = 11 cells, p = 0.125, Kruskal-

1267 Wallis test;; ii) rank order plot and linear regression fit; slope = 1.01, intercept = 1.53, R^2 = 0.97;
1268 iii) ratio plot, TTX mEPSC amplitude/CON mEPSC amplitude vs. CON mEPSC amplitude. Gray
1269 line, identity; red dashed line, linear regression fit. Insets in rank order plots depict full range of
1270 data.

1271

1272

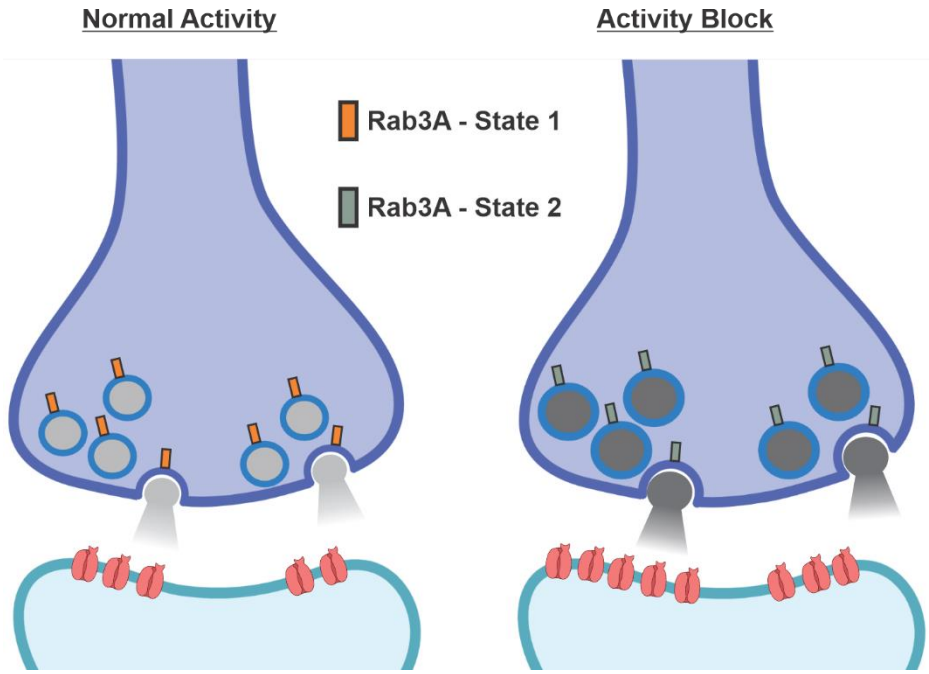

FIGURE 10

Figure 10. Rab3A is required for increased mEPSC amplitude after activity blockade via 2 mechanisms: 1. increased amount of transmitter released from a single vesicle and 2. increased postsynaptic receptors. *Left*: in the presence of normal activity, Rab3A is in its control state ("State 1," red), maintaining mEPSC amplitude within a limited range by regulating either vesicle size or transmitter content, or both, and by regulating the number of postsynaptic receptors, likely through release of an anterograde signal. *Right*: after activity is blocked, Rab3A accumulates in an alternate functional state ("State 2," gray) resulting in quantal size expanding to larger ranges because of increased vesicle size or transmitter content and because of increased numbers of receptors no longer being under the normal control of the anterograde signal.

	Rab3A$^{+/+}$		**Rab3A$^{-/-}$**	
mEPSC amplitude (pA)	**CON**	**TTX**	**CON**	**TTX**
mean	13.7 ± 4.5 (n=23)	16.4 ± 4.3 (n=24)	14.9 ± 3.8 (n=21)	14.0 ± 4.0 (n=19)
KW p value	p = 0.016		p = 0.34	
KS comparison of CDF	N CON (n=690), N TTX (n=720) D = 0.162 p = 1.42 * 10^{-8}		N CON (n=630), N TTX (n=570) D = 0.072 p= 0.085	
Rank order linear regression (slope, intercept, R^2)	Slope, 1.11 Intercept, 1.22 R^2, 0.984		Slope, 0.93 Intercept, 0.13 R^2, 0.997	
Mean ratio TTX/CON 50-75th quantile	1.24		0.957	
GluA2 receptor cluster size (μm^2)	**CON**	**TTX**	**CON**	**TTX**
mean	0.97 ± 0.38 (n=29)	1.15 ± 0.59 (n=29)	0.93 ± 0.27 (n=30)	0.91 ± 0.28 (n=29)
KW p value	p = 0.44		p = 0.74	
KS comparison of CDF	N CON (n=870), N TTX (n=870) D = 0.089 p = 0.002		N CON (n=900), N TTX (n=870) D = 0.045 p = 0.31	
Rank order linear regression (slope, intercept, R^2)	Slope, 1.33 Intercept, -0.13 R^2, 0.98		Slope, 1.01 Intercept, -0.03 R^2, 0.993	
Mean ratio TTX/CON 50-75th quantile	1.11		0.976	
GluA2 receptor cluster intensity (arb. units)	**CON**	**TTX**	**CON**	**TTX**
mean	673 ± 90 (n=29)	687 ± 72 (n=29)	766 ± 68 (n=30)	776 ± 79 (n=29)
KW p value	p = 0.25		p = 0.47	
KS comparison of CDF	N CON (n=870), N TTX (n=870) D = 0.120 p = 6.73 * 10^{-6}		N CON (n=900), N TTX (n=870) D = 0.060 p = 0.08	
Rank order linear regression (slope, intercept, R^2)	Slope, 0.90 Intercept, 82 R^2, 0.987		Slope, 1.09 Intercept, -60 R^2, 0.993	
Mean ratio TTX/CON 50-75th quantile	1.02		1.02	

TABLE 1

1301 Table 1. Comparison of effect of activity blockade with TTX on mEPSC amplitude and GluA2 receptor
1302 cluster characteristics. Voltage clamp recordings of mEPSCs and confocal imaging of GluA2 receptor
1303 immunofluorescence at VGLU1-positive synapses were performed on coverslips from the same 3
1304 Rab3A$^{+/+}$ cultures (left) and 3 Rab3A$^{-/-}$ cultures (right). p values are not corrected for multiple
1305 comparisons.